Gradual Increase in Environmental Light Intensity Induces Oxidative Stress and Inflammation and Accelerates Retinal Neurodegeneration

Oksana Kutsyr,[1] Xavier Sánchez-Sáez,[1] Natalia Martínez-Gil,[1] Emilio de Juan,[1] Pedro Lax,[1] Victoria Maneu,[2] and Nicolás Cuenca[1,3]

[1]Department of Physiology, Genetics and Microbiology, University of Alicante, Alicante, Spain
[2]Department of Optics, Pharmacology and Anatomy, University of Alicante, Alicante, Spain
[3]Institute Ramón Margalef, University of Alicante, Alicante, Spain

Correspondence: Nicolás Cuenca, Department of Physiology, Genetics and Microbiology, University of Alicante, San Vicente del Raspeig, E-03080 Alicante, Spain; cuenca@ua.es.

Received: March 25, 2020
Accepted: July 6, 2020
Published: August 3, 2020

Citation: Kutsyr O, Sánchez-Sáez X, Martínez-Gil N, et al. Gradual increase in environmental light intensity induces oxidative stress and inflammation and accelerates retinal neurodegeneration. *Invest Ophthalmol Vis Sci.* 2020;61(10):1. https://doi.org/10.1167/iovs.61.10.1

Purpose. Retinitis pigmentosa (RP) is a blinding neurodegenerative disease of the retina that can be affected by many factors. The present study aimed to analyze the effect of different environmental light intensities in rd10 mice retina.

Methods. C57BL/6J and rd10 mice were bred and housed under three different environmental light intensities: scotopic (5 lux), mesopic (50 lux), and photopic (300 lux). Visual function was studied using electroretinography and optomotor testing. The structural and morphological integrity of the retinas was evaluated by optical coherence tomography imaging and immunohistochemistry. Additionally, inflammatory processes and oxidative stress markers were analyzed by flow cytometry and western blotting.

Results. When the environmental light intensity was higher, retinal function decreased in rd10 mice and was accompanied by light-dependent photoreceptor loss, followed by morphological alterations, and synaptic connectivity loss. Moreover, light-dependent retinal degeneration was accompanied by an increased number of inflammatory cells, which became more activated and phagocytic, and by an exacerbated reactive gliosis. Furthermore, light-dependent increment in oxidative stress markers in rd10 mice retina pointed to a possible mechanism for light-induced photoreceptor degeneration.

Conclusions. An increase in rd10 mice housing light intensity accelerates retinal degeneration, activating cell death, oxidative stress pathways, and inflammatory cells. Lighting intensity is a key factor in the progression of retinal degeneration, and standardized lighting conditions are advisable for proper analysis and interpretation of experimental results from RP animal models, and specifically from rd10 mice. Also, it can be hypothesized that light protection could be an option to slow down retinal degeneration in some cases of RP.

Keywords: lighting intensity, retinitis pigmentosa, rd10, oxidative stress, inflammation

Retinitis pigmentosa (RP) is a very heterogeneous group of inherited neurodegenerative diseases of the retina that affect the structure and function of photoreceptors and retinal pigment epithelium (RPE). This group of diseases is characterized by the progressive loss of vision from the periphery toward the central retina, known as tunnel vision, eventually leading to complete blindness.[1–3] The disease begins with a primary degeneration of rod photoreceptors, followed by a secondary dysfunction of cone photoreceptors. To date, mutations have been identified in more than 80 different genes that can lead to RP.[4] More than half of those mutations are located in genes that encode proteins related to the phototransduction cascade.[5] In rd10 mice, one of the most used animal models of RP, retinal degeneration is caused by a missense mutation in exon 13 of the catalytic b subunit of the phosphodiesterase 6 (*Pde6b*) gene,[6] which is involved in the hydrolysis of cyclic guanosine monophosphate (cGMP). Pde6b mutation causes an increase in cGMP concentration, affecting cGMP-gated channels and the flow of cations through them,[7–9] inducing rod photoreceptor degeneration, which leads to secondary cone photoreceptor death. As a consequence of this photoreceptor cell death, there is an increase of the retinal inflammatory state due to the activation of microglia, which also exacerbates retinal degeneration.[10]

Many studies suggest that the death of rod photoreceptors is accompanied by an increase of retinal oxygen levels[11] and reactive oxygen species (ROS) from different sources.[12,13] This contributes to the increment of oxidative stress and exacerbates rod degeneration.[14–18] It is known that, in a stress context, ROS may interact with macromolecules, including lipids, proteins, or DNA, inducing cell dysfunction and death.[19,20] In addition, the retina has a high level of nitric oxide (NO), a widespread neurotransmitter in this tissue.[21,22] However, NO may also interact with oxygen and superoxide anion, generating reactive nitrogen

species (RNS) and peroxynitrite, which are extremely neurotoxic.[21–23]

Although continuous light deprivation has been proposed as a potential factor to prevent retinal degeneration in RP,[20,24–27] the retinal daily exposure to light is almost inevitable in patients. Thus, the effect of light on retinal degeneration remains an important issue to be considered. In this work, we focus on the effects of three different light intensities, corresponding to scotopic, mesopic, and photopic vision, on retinal degeneration in rd10 mice and healthy animals. Our results indicate that an increase of environmental light intensity is determinant for the progression of the retinal degeneration in RP and related diseases.

Material and Methods

Animals and Light Conditions

Male and female C57BL/6J and homozygous rd10/rd10 (B6.CXBl-Pde6b^{rd10}/J) mice, both pigmented, were used. All mice were bred and provided by the animal facility of the University of Alicante, and they were kept under controlled conditions of temperature (23 ± 1°C) and humidity (55%–60%). The animals were kept in transparent polysulfone cages and exposed to a cycle of 12 hours light/12 hours darkness. Three different environmental light conditions were tested: scotopic (5 lux), mesopic (50 lux), and photopic (300 lux), using natural daylight fluorescent tubes as a light source. The light intensity was measured at the cage level with the light sensor oriented toward the light source using a Mavolux Digital Lux Meter (GOSSEN Foto- und Lichtmesstechnik GmbH, Nuremberg, Germany). All animals were born under mesopic conditions and moved to darker or brighter conditions before postnatal day 10 (P10), prior to eye-opening. A total of 62 mice were used, distributed in six experimental groups: rd10 mice raised at 5 lux (n = 11), 50 lux (n = 11), or 300 lux (n = 12) and age-matched wild-type C57BL/6J mice also raised at 5 lux (n = 8), 50 lux (n = 8), or 300 lux (n = 12). At the end of the experiment (P30), all animals were euthanized by cervical dislocation.

All animals were handled and maintained following the current ARVO Statement for the Use of Animals in Ophthalmic and Vision Research and European Directive 2010/63/EU. The experiments were approved by the research ethics committee for animal use and care at the University of Alicante (UA-07/22/2013). All effort was taken to minimize animal suffering and to reduce the number of animals used.

PCR and Rpe65 Sequence Analysis

The existence of the *Rpe65 Leu$_{450}$Met* gene variation, found in the C57BL/6J mouse genome,[28] confers resistance against light damage.[29] To corroborate the existence of this polymorphism in our experimental groups, total genomic DNA was isolated from C57BL/6J and rd10 mice tail tissue using the NucleoSpin Tissue kit (Macherey-Nagel GmbH & Co. KG, Dueren, Germany). The region of interest of the *Rpe65* gene was amplified by PCR using HOT FIREPol DNA Polymerase (Solis BioDyne, Tartu, Estonia) and specific primers (forward, 5′-TATGCATACGGACTTGGGTTGA-3′; reverse, 5′-TTCTGGTGCAGTTCCATTCAGT-3′) designed using the Primer designing tool (National Center for Biotechnology Information, Bethesda, MD, USA). The PCR was performed under the following conditions: one 15-minute initial denaturing step at 95°C; 30 cycles of a 20-second denaturing step at 95°C; a 24-second annealing step at 63°C; a 42-second elongation step at 72°C; and one 5-minute final elongation step at 72°C. This amplification resulted in a product of 391 bp purified with the NZYGelpure kit (NZYTech, Lisboa, Portugal) and sent to Sanger sequencing (STAB Vida, Caparica Portugal).

Electroretinograph Recordings

Electroretinography (ERG) responses were recorded in total darkness at P30, after overnight adaptation to darkness. The animals were anesthetized by an injection of ketamine (100 mg/kg) and xylazine (4 mg/kg), kept on a thermal blanket at 38°C, and prepared for bilateral recording under dim red light. The pupils were dilated by 1% tropicamide (Alcon Cusí, Barcelona, Spain) and 0.2% polyacrylic acid carbomer (Viscotears; Novartis, Barcelona, Spain) was instilled to improve the electric contact and to avoid eye dehydration. DTL fiber electrodes (Retina Technologies, Scranton, PA, USA) were used for recording. As a reference electrode, a 25-G platinum needle was inserted under the scalp between the eyes. A ground needle electrode was inserted under the skin in the base of the tail. All of the procedure was performed in a Faraday cage. Scotopic ERG responses were recorded in both eyes with a Ganzfeld illuminator generating flashlight stimuli. Eleven stimuli with increasing luminance of 10-ms duration were presented to the animals. An interval of 10 seconds was left between dim flashes (–5 to –0.6 log cd·s/m^2) and 20 seconds between the highest flashes (0–1 log cd·s/m^2). Using a DAM50 data acquisition board (World Precision Instruments, Aston, UK), signals were amplified and band-filtered (1–1000 Hz, without notch filtering). A PowerLab system (AD Instruments, Oxfordshire, UK) was used to perform stimuli presentation and data acquisition (4 kHz). The amplitude of the a-wave was measured from the prestimulus baseline to the most negative trough, and the amplitude of the b-wave was measured from the trough of the a-wave to the peak of the b-wave.

Optomotor Test

An Argos optomotor system (Instead Technologies, Elche, Spain) was used to evaluate the visual acuity of awake, freely moving mice at the endpoint (P30). The system is comprised of a chamber formed by four computer screens facing each other and a central platform on which to place the mice (Fig. 2E). The stimuli consisted of vertically oriented gratings that rotate horizontally around the animal for 5 seconds, with an initial spatial frequency of 0.088 cycles/degree and 100% contrast. The mouse response was recorded by a camera located in the upper part of the system. Smooth head movements in the direction of the rotating gratings were evaluated by a trained observer. The visual acuity threshold was assigned to the last spatial frequency to which the mouse responded.

Optical Coherence Tomography

High-resolution optical coherence tomography (OCT) images of the central retina were obtained with a Spectralis OCT system (Heidelberg Engineering, Heidelberg, Germany). The animals were anesthetized through

Investigative Ophthalmology & Visual Science

Table. Antibodies Used for Immunofluorescence and Western Blotting

Molecular Marker	Antibody	Supplier	Catalog No.	Dilution
Cone arrestin	Rabbit polyclonal	MilliporeSigma	AB15282	IF 1:200
Rhodopsin	Mouse monoclonal	MilliporeSigma	MAB5356	IF 1:100
Calbindin D-28K	Rabbit polyclonal	Swant	CB-38a	IF 1:500
C-terminal binding protein-2 (CtBP2)	Mouse monoclonal	BD Biosciences	612044	IF 1:1000
Vesicular glutamate transporter 1 (VGluT1)	Guinea Pig polyclonal	MilliporeSigma	AB5905	IF 1:1000
Ionized calcium-binding adapter molecule 1 (Iba1)	Rabbit polyclonal	Wako Chemicals	019-19741	IF 1:1000
Glial fibrillary acidic protein (GFAP)	Mouse monoclonal	Sigma-Aldrich	G3893	IF 1:500
CD68	Rat monoclonal	Bio-Rad Laboratories	MCA1957	IF 1:500
4-Hydroxynonenal (4-HNE)	Mouse monoclonal	Abcam	ab48506	WB 1:1000
Nitric oxide synthase 1 (NOS1) antibody R-20	Rabbit polyclonal	Santa Cruz Biotechnology	sc-648	WB 1:200
Recoverin	Rabbit polyclonal	MilliporeSigma	AB5585	WB 1:1000
Glyceraldehyde-3-phosphate dehydrogenase (GAPDH)	Mouse monoclonal	MilliporeSigma	MAB374	WB 1:500

Supplier locations: MilliporeSigma (Burlington, MA, USA); Swant (Marly, Switzerland); BD Biosciences (San Jose, CA, USA); Wako (Richmond, VA, USA); Sigma-Aldrich (St. Louis, MO, USA); Bio-Rad Laboratories (Hercules, CA, USA); Abcam (Cambridge, UK); Santa Cruz Biotechnology (Santa Cruz, CA, USA). IF, immunofluorescence; WB, western blotting.

intraperitoneal injection of ketamine (100 mg/kg) and xylazine (4 mg/kg) and were kept on a heating pad at 38°C. The pupils were dilated by topical application of 1% tropicamide (Alcon Cusí). In order to preserve corneal hydration, a drop of physiological serum was applied in each eye and protected by a contact lens. OCT high-resolution cross-sectional images were generated in the central region of the retina, above the optic nerve. Total retinal thickness excluding RPE was quantified throughout the OCT cross-sectional images in six different points separated by 500 µm. Four to 12 animals were analyzed in each experimental group.

Immunohistochemistry

All histological studies were performed at P30. After sacrificing the animals, the dorsal margin of the limbus was marked by a suture. The eyes were enucleated and fixed at room temperature in 4% paraformaldehyde (PFA) for 1 hour, washed in 0.1-M phosphate buffer (PB; pH 7.4), and sequentially cryoprotected in 15%, 20%, and 30% (w/v) sucrose. Cornea, lens, and vitreous body were removed, and the eyecups were prepared for cross-sectional cryosections as previously described by our group.[30–32] Sections 16-µm thick were obtained and stored at –20°C.

For single or double immunostaining procedure, sections were thawed, washed in PB, and incubated 1 hour in blocking solution, consisting of 10% (v/v) normal donkey serum in PB with 0.5% Triton X-100 (Sigma-Aldrich, St. Louis, MO). The sections were then incubated overnight at room temperature with the appropriate combinations of primary antibodies at different dilutions (listed in the Table) in PB with 0.5% Triton X-100. Sections were then washed in PB and incubated with the secondary antibodies for 1 hour. Secondary antibodies used were Molecular Probes Anti-Rabbit Alexa Fluor 488 and 555, Anti-Mouse Alexa Fluor 555 and 647, Anti-Guinea Pig Alexa Fluor 633, and Anti-Rat Alexa Fluor 488 conjugates (1:100; Thermo Fisher Scientific, Waltham, MA, USA). When indicated, the Molecular Probes nuclear marker TO-PRO-3 iodide was added at a 1:1000 dilution. Finally, sections were washed in PB and mounted with Citifluor (Citifluor Ltd., London, UK) under a coverslip. Images were taken with a Leica TCS SP8 confocal laser-scanning microscope (Leica Microsystems, Wetzlar, Germany).

To quantify the number of photoreceptor rows, hematoxylin staining was performed. For this purpose, sections were thawed, washed in PB, and stained with Mayer's hematoxylin solution (254766; Panreac, Barcelona, Spain) for 5 minutes. Then, sections were washed and mounted with glycerol:PB (1:1 v/v) solution under a coverslip. The number of photoreceptor rows was measured in at least two non-consecutive sections containing the optic nerve in three to seven retinas from each experimental group. The quantification was performed every 500 µm from the optic nerve to each ora serrata (temporal and nasal).

Quantification of Synaptic Connectivity

In order to evaluate synaptic connectivity between photoreceptors and their postsynaptic cells, the fluorescence area associated with C-terminal binding protein 2 (CtBP2) immunostaining in the outer plexiform layer (OPL) was measured using ImageJ software (National Institutes of Health, Bethesda, MD, USA). The quantification was carried out in central images taken on each side of the optic nerve, in at least three non-consecutive sections.

Quantification of Inflammation Markers

Different markers were used to measure the inflammatory state of the retinas in animals of both strains under the different housing light conditions (5, 50, or 300 lux). Cross-sectional retinal cryosections were used to quantify the number of microglial cells (ionized calcium-binding adapter molecule 1 [Iba1] positive),[33,34] as well as the microglial cells that expressed the CD68 marker (specific for a phagocytic state).[34,35] The quantification was performed in at least four non-consecutive sections, and the total length of the retinal sections was analyzed.

In addition, gliosis in Müller cells and astrocytes was analyzed measuring the fluorescence area associated with glial fibrillary acidic protein (GFAP) immunostaining using the ImageJ software. The quantification was performed on central images taken on each side of the optic nerve, in at least three non-consecutive sections.

Flow Cytometry

The immune system-related cell populations in the retinas were analyzed using flow cytometry. After the eyes were enucleated, retinas were dissected out and disaggregated

in 1 mL of pH 7.4 PBS by pipetting gently up and down, using a wide-bore pipette tip. Then, retinal cell suspensions were filtered, to prevent clumps, using a 30-µm strainer (BD Biosciences, San Diego, CA, USA), and labeled with a cocktail of five antibodies acquired from e-Bioscience (San Diego, CA, USA): anti-CD11b-PE (clone M/170), anti-CD45-FITC (clone 30-F11), anti-CD11c-PerCpCy5.5 (clone N418), anti-major histocompatibility complex (MHC) class II (I-A/I-E)-PECy7 (clone M5/114.15.2), and anti-CD169-eFluor 660 (clone SER-4). After discarding doublets and debris events, the CD11b-positive cells (a marker of myeloid cells, as microglia and infiltrating macrophages)[36–38] were analyzed for their immunoreactivity against MHC class II (activated cells),[39–41] CD11c (a marker of dendritic and microglia cell populations),[42–44] and sialoadhesin (CD169, which stains activated macrophages and microglial cell populations).[45,46] Immunoreactivity against CD169, CD11c, and MHC class II antibodies in CD11b-positive cells allowed analysis of subpopulations of cells that contribute to the inflammatory process, as do the activated microglia and infiltrating cells. The immunogenicity against CD45 was also analyzed as a marker of the microglia and leucocyte population, which is increased in activated cells, infiltrating monocytes and macrophages.[38,41,47] Each mouse retina was analyzed individually, and at least three retinas from different animals for each experimental group were assessed. Data were acquired on an LSR Fortessa cytometer (BD Biosciences) and analyzed using FCS Express 6 flow cytometry software (De Novo, Los Angeles, CA, USA).

Western Blot

Retinas were isolated and proteins were extracted using RIPA buffer (Sigma-Aldrich) containing protease (cOmplete EDTA-free; Roche Applied Science, Mannheim, Germany) and phosphatase (PhosStop; Roche) inhibitor cocktails. After incubation for 30 minutes, debris was pelleted by 10-minute centrifugation (14,000*g*) at 4°C, and protein concentration in the supernatants was quantified with the Bio-Rad protein assay (Bio-Rad Laboratories, Inc., Hercules, CA, USA), using bovine serum albumin as standard. Equal amounts of protein from each sample (40 µg) were denatured by diluted in Laemmli Sample Buffer (4% SDS, 100-mM dithiothreitol, 20% glycerol, 0.004% bromophenol blue, 125-mM Tris-HCl, pH 6.8; Bio-Rad Laboratories) and heated to 95°C for 10 minutes. Afterward, samples were resolved on 5% to 12% SDS-PAGE gels and transferred onto polyvinylidene difluoride membranes (MilliporeSigma, Burlington, MA, USA). Membranes were incubated overnight at 4°C with 4-hydroxynonenal (4-HNE), neuronal nitric oxide synthase (nNOS), recoverin (RCVRN), and glyceraldehyde-3-phosphate dehydrogenase (GAPDH) (Table) antibodies prepared in 2.5% (w/v) non-fat dry milk in Tris-buffered saline/0.1% Tween-20 (TBS/T, pH 7.6). After three 5-minute washes with TBS/T, membranes were incubated for 2 hours at room temperature with Invitrogen goat anti-rabbit or goat anti-mouse IgG–horseradish peroxidase (1:5000; Thermo Fisher Scientific) in TBS/T. Thereafter, the blots were washed again with TBS/T and incubated with Pierce ECL substrate (Thermo Fisher Scientific). The signal was revealed and detected with a ChemiDoc XRS+ imaging system (Bio-Rad Laboratories). Finally, protein levels were quantified by densitometry using ImageJ software and normalized by GAPDH values as a housekeeping protein.

Superoxide Anions Production

Dihydroethidium (DHE, D1168; Thermo Fisher Scientific), a redox-sensitive probe that exhibits bright red fluorescence in the cell cytoplasm and nucleus when oxidized to ethidium, was used to quantify the state of oxidative stress. Briefly, isolated whole-mount retinas were incubated with 5-µM DHE in Dulbecco's Modified Eagle Medium/Nutrient Mixture F-12 (DMEM/F-12) for 30 minutes at 37°C and 5% CO_2. Then, after three washes in PB solution, retinas were fixed in 4% PFA for 30 minutes. Images were taken with a Leica TCS SP8 confocal laser-scanning microscope (Leica Microsystems). The number of cells that presented intracellular oxidized DHE was counted and relativized to the area in at least four images taken from different regions of whole-mounted retinas.

Statistics

Data for C57BL/6J and rd10 mice reared at the three different light conditions were statistically analyzed using Prism software (GraphPad Software, Inc., San Diego, CA, USA). The D'Agostino–Pearson normality test was used to determine whether the data followed a normal distribution. For data with a normal distribution, ANOVAs and Tukey's post hoc tests were applied to determine the significant differences between the different experimental groups. By contrast, for data without a normal distribution, Kruskal–Wallis and Dunn's post hoc tests were applied. When two groups were compared, the Mann–Whitney *U* test was applied. Differences were considered statistically significant at $P < 0.05$. Values in all graphs were represented as the mean value ± SEM.

Results

C57BL/6J and rd10 Mice Present a Protective Polymorphism in *Rpe65* Gene

To ascertain the presence of the *Rpe65* $Leu_{450}Met$ gene variation in our experimental groups, a region of the exon 13 that include the codon of interest was targeted (Fig. 1A). After extraction of genomic DNA from C57BL/6J and rd10 mice tissue, the target region was amplified by PCR and the product was purified and sequenced. Both C57BL/6J and rd10 mice carried the polymorphism that confers resistance against light-induced damage, presenting the ATG (Met) variant in the 450 codon of the *Rpe65* gene instead of the CTG (Leu) codon (Figs. 1B, 1C).

Light-Induced Alterations of Visual Responsiveness

In order to assess the effect of environmental light on the visual function of normal and diseased retinas, scotopic ERG responses were recorded in both C57BL/6J and rd10 mice at P30. In all three experimental conditions tested, ERG amplitudes in C57BL/6J (Fig. 2A) were higher than those obtained in rd10 mice at the same light conditions (Fig. 2B). No differences in the amplitude of ERG responses were found between C57BL/6J mice reared at different environmental light conditions (Fig. 2C). By contrast, in rd10 mice, a significant light-dependent decrease in the amplitude of both a- and b-waves was observed for almost all flash luminances (Fig. 2D). Mean values of a- and b-wave amplitudes

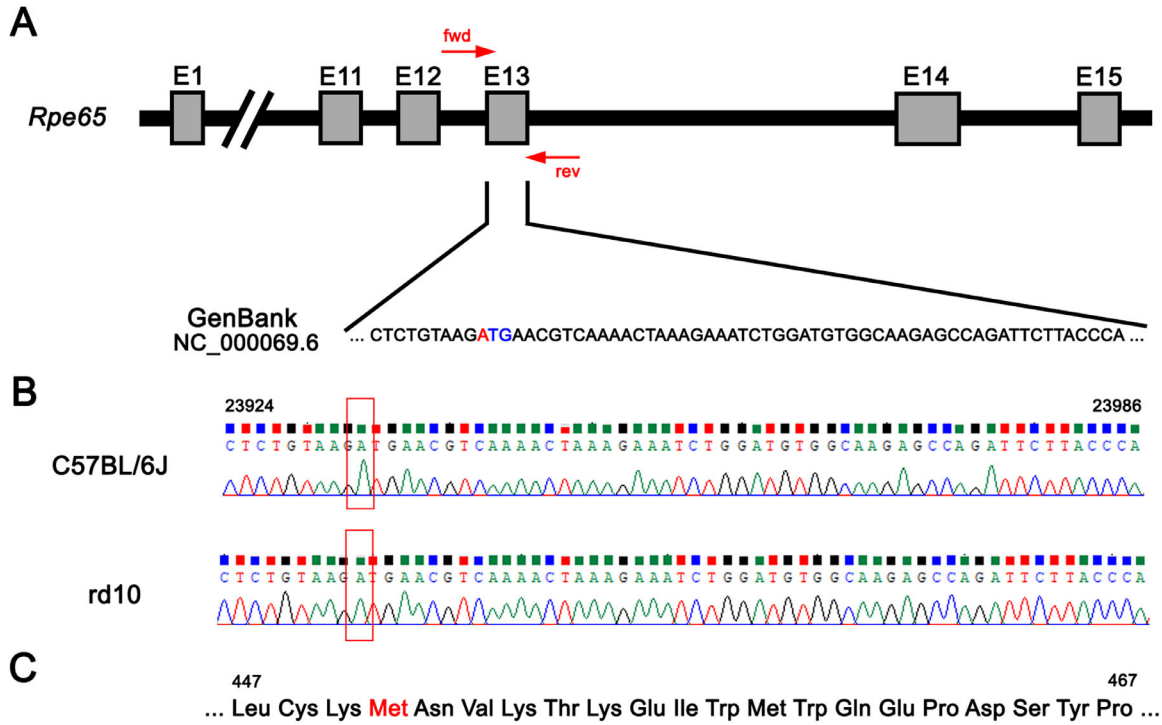

Figure 1. C57BL/6J and rd10 mice present the Rpe65 Leu450Met variant. (**A**) A schematic representation of the *Rpe65* gene and its exons. The forward and reverse primers (forward, 5′-TATGCATACGGACTTGGGTTGA-3′; reverse, 5′-TTCTGGTGCAGTTCCATTCAGT-3) flank the regions of interest, which include codon 450 in the exon 13 (*red* and *blue*). The C57BL/6J mice genome, found in DNA databases (GenBank; NC_000069.6), presents the polymorphism (*red nucleotide*) that confers light-induced damage resistance. (**B**) For C57BL/6J and rd10 mice, Sanger sequencing results of PCR products after genomic amplification of the region of interest. Boxed region corresponds to the polymorphism. (**C**) Segment of the RPE65 amino acid sequence highlighting the 450 amino acid (Met) in *red*.

from rd10 mice reared at 300 lux were significantly lower (41% and 68% of decrease at the higher flash intensity) than those measured in rd10 mice reared at 50 lux ($P < 0.0001$, both waves) (Figs. 2C, 2D). In the same way, mean values of a- and b-wave amplitudes from rd10 mice maintained at 50 lux were significantly lower (73% and 48% of decrease at the higher flash intensity) than those obtained in rd10 mice reared at 5 lux ($P < 0.05$ and $P < 0.0001$ for the respective waves) (Figs. 2C, 2D).

Optomotor testing was performed to analyze visual acuity in both strains in the three light conditions. No differences were found among the three C57BL/6J mice groups (Fig. 2F). However, visual acuity values for rd10 mice housed at 5-, 50-, and 300-lux cyclic light were significantly lower than the values for their matching C57BL/6J animals (48%, 66%, and 79% lower, respectively). Also, a light-dependent visual acuity reduction was observed in the rd10 strain, where animals reared at 300 lux showed the lowest values. Mean values from rd10 mice reared at 300 lux were significantly lower than those from rd10 mice reared at 50 lux (37% less; $P < 0.001$), and these were significantly lower than the ones obtained in animals reared at 5 lux (35% less; $P < 0.0001$) (Fig. 2F). Altogether, these results demonstrate that an increase in the rearing light intensity induces a decrease in retinal responsiveness in rd10 mice.

Light-Induced Degeneration of Photoreceptor Population

In order to assess the integrity of the retina, OCT images were obtained at P30 from C57BL/6J and rd10 mice reared in different light conditions. Figure 3 shows representative OCT images (Figs. 3A–3F) and retinal thickness measurements (Fig. 3G) from each experimental group. In C57BL/6J mice housed at the different conditions, there were no differences in the retinal structure (Figs. 3A–3C) or in the mean retinal thickness (Fig. 3G), indicating that, under our experimental conditions, rearing light intensity does not affect the integrity of the retina in healthy animals. Conversely, in rd10 mice, a higher decrease in the total retinal thickness was observed as the light environment increased (Figs. 3D–3F), which is probably due to the degeneration of photoreceptors. However, due to a disorganization of the outer hyper- and hyporeflective layers in rd10, it was not possible to accurately measure the outer nuclear layer (ONL) thickness in these animals. OCT images of rd10 mice reared at 5 lux still showed the outer hyperreflective band corresponding to the ellipsoid zone, which became fainter in rd10 mice reared at 50 lux and completely disappeared in rd10 mice housed at 300 lux, for which it was not possible to distinguish any band. Finally, statistically significant differences in the total retinal thickness were found between the rd10 5-lux and 300-lux groups ($P < 0.05$) and between the rd10 50-lux and 300-lux groups ($P = 0.005$), with the 300-lux intensity being the environmental condition where a major decrease in retinal thickness occurred (Fig. 3G).

The number of photoreceptor rows in the retinas of each experimental group was quantified in cross-sectional cryosections stained with hematoxylin (Figs. 4A–4F). As the progression of the retinal degeneration in the rd10 mice model is not uniform throughout the retina, the number of photoreceptor rows was quantified in different retinal areas,

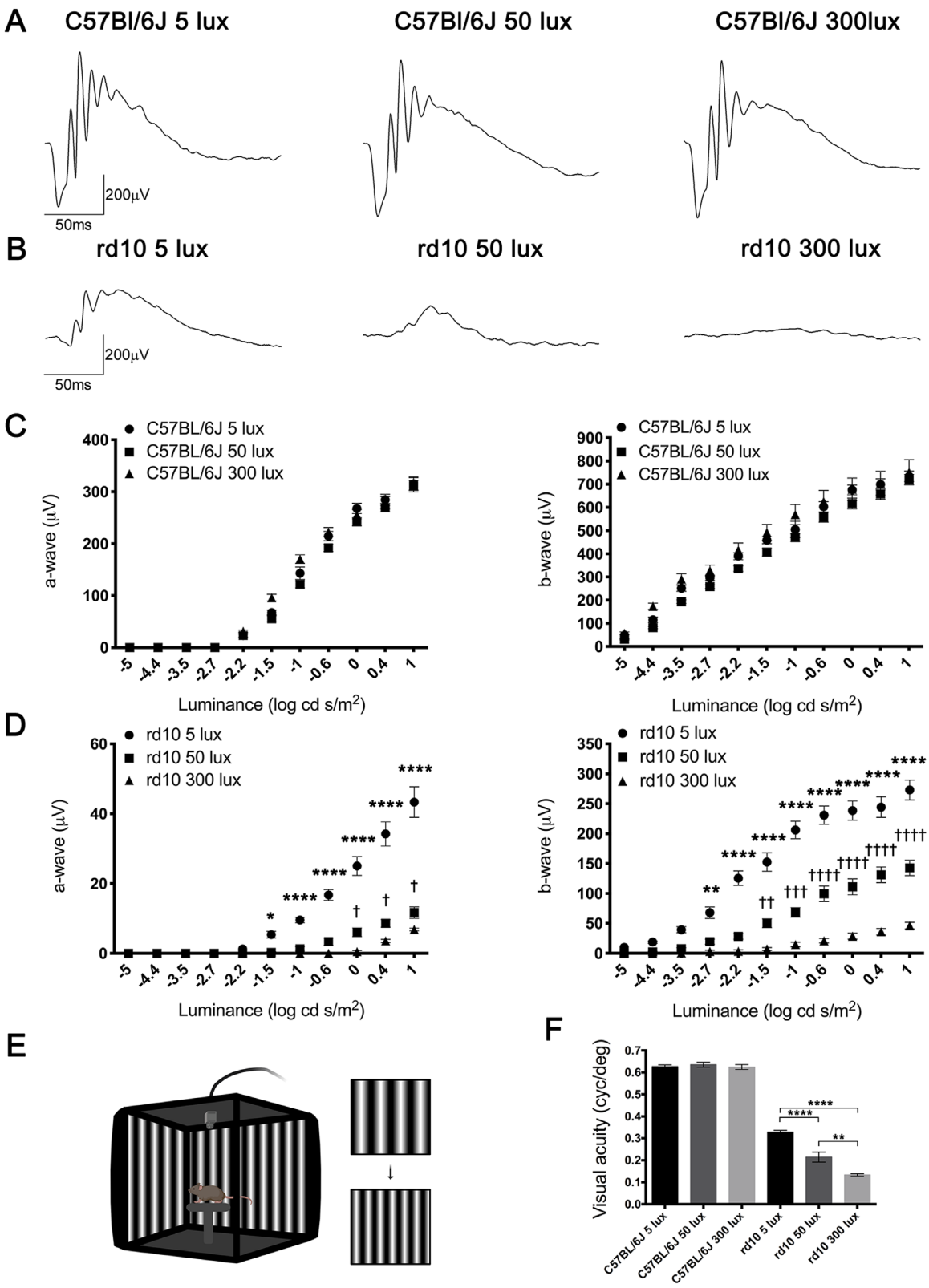

Figure 2. Effect of environmental light conditions on retinal function. (**A**, **B**) Representative dark-adapted ERG intensity responses to 1 log cd·s/m^2 flashes from C57BL/6J (**A**) and rd10 mice (**B**) reared under 5, 50, and 300 lux cyclic light. (**C**, **D**) Luminance–response curves of P30 C57BL/6J (**C**) and rd10 mice (**D**) housed at the different light conditions (n = 5 to 9). Each graph includes measurements for mixed a-wave (*left graphs*) and b-wave (*right graphs*) responses. (**E**) Configuration of the optomotor system. Image was created using BioRender (https://biorender.com/). (**F**) Visual acuity measured as the spatial frequency threshold in C57BL/6J and rd10 mice reared at 5, 50, and 300 lux (n = 4 to 9). Two-way (ERG) and one-way (optomotor test) ANOVA and Tukey's post hoc test. $^{*}P < 0.05$, $^{**}P < 0.01$, $^{***}P < 0.001$, $^{****}P < 0.0001$ for comparisons between animals housed at 50 and 300 lux. $^{\dagger}P < 0.05$, $^{\dagger\dagger}P < 0.01$, $^{\dagger\dagger\dagger}P < 0.001$, $^{\dagger\dagger\dagger\dagger}P < 0.0001$ for comparisons between animals housed at 5 and 50 lux.

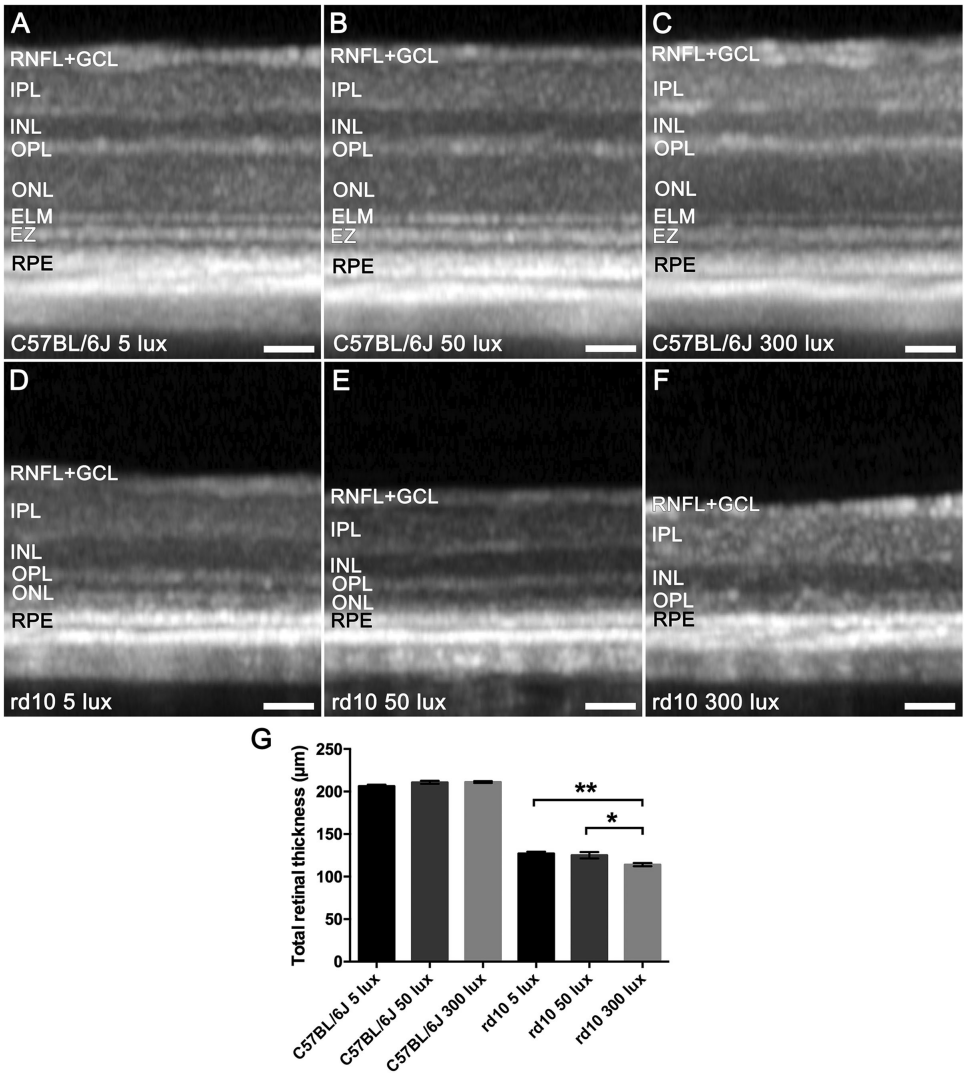

Figure 3. Effect of environmental light conditions on retinal structure. (**A–F**) OCT images of P30 C57BL/6J mice (**A–C**) and rd10 mice (**D–F**) maintained under 5, 50, and 300 lux cyclic light. (**G**) Mean total retinal thickness quantification ($n = 4$ to 12). Kruskal–Wallis test (for C57BL/6J mice); one-way ANOVA, Tukey's post hoc test (for rd10 mice). $^{*}P < 0.05$, $^{**}P < 0.01$. RNFL+GCL, retinal nerve fiber layer and ganglion cell layer; IPL, inner plexiform layer; INL, inner nuclear layer; OPL, outer plexiform layer; ONL, outer nuclear layer; ELM, external limiting membrane; EZ, ellipsoid zone; RPE, retinal pigment epithelium. *Scale bars*: 50 µm.

from the temporal to the nasal zone (Figs. 4G, 4H). No significant differences were found in the mean number of photoreceptor rows among C57BL/6J mice exposed to the three housing light conditions studied (Fig. 4G), but there was a slight decrease in the mean photoreceptor rows from the center to the periphery. In contrast, rd10 mice at the same age showed a drastic reduction in the number of photoreceptor rows. Also, the degeneration was not uniform throughout the retina, being more pronounced in the temporal zone in all rd10 mice experimental groups, regardless of the rearing light intensity (Fig. 4H). Moreover, rd10 mice exhibited a light-dependent photoreceptor degeneration, where rd10 mice reared at 5 lux showed the highest number of photoreceptor rows in the central, temporal, and nasal zone (3.4 ± 0.2, 5.0 ± 0.4, and 6.5 ± 0.6, respectively), and the rd10 mice reared at 300 lux showed the lowest number of photoreceptor rows (1.0 ± 0.0, 2.4 ± 0.2, and 3.6 ± 0.1, at the same zones).

Because OCT images showed anomalies in the hyperreflective bands of the outer retina of rd10 mice, specific markers were used to study photoreceptor morphology in both strains (Fig. 5). No differences in photoreceptor morphology were observed between C57BL/6J mice housed under the different light-rearing conditions (Figs. 5A–5C). In all cases, normal cone photoreceptors (green) with well-defined outer segments, long axons, and normal pedicles were observed. Furthermore, all of the C57BL/6 mice groups exhibited a normal rhodopsin distribution (red), located in the rod outer segments. By contrast, striking differences in the photoreceptor morphology were observed among the three rd10 mice groups (Figs. 5D–5F), compared with C57BL/6J mice. Moreover, photoreceptor degeneration in rd10 mice varied with light intensity (5, 50, and 300 lux). The distribution of rhodopsin in rd10 mice rod cells was abnormal. In these mice, rhodopsin was no longer completely located in the rod outer segments but was

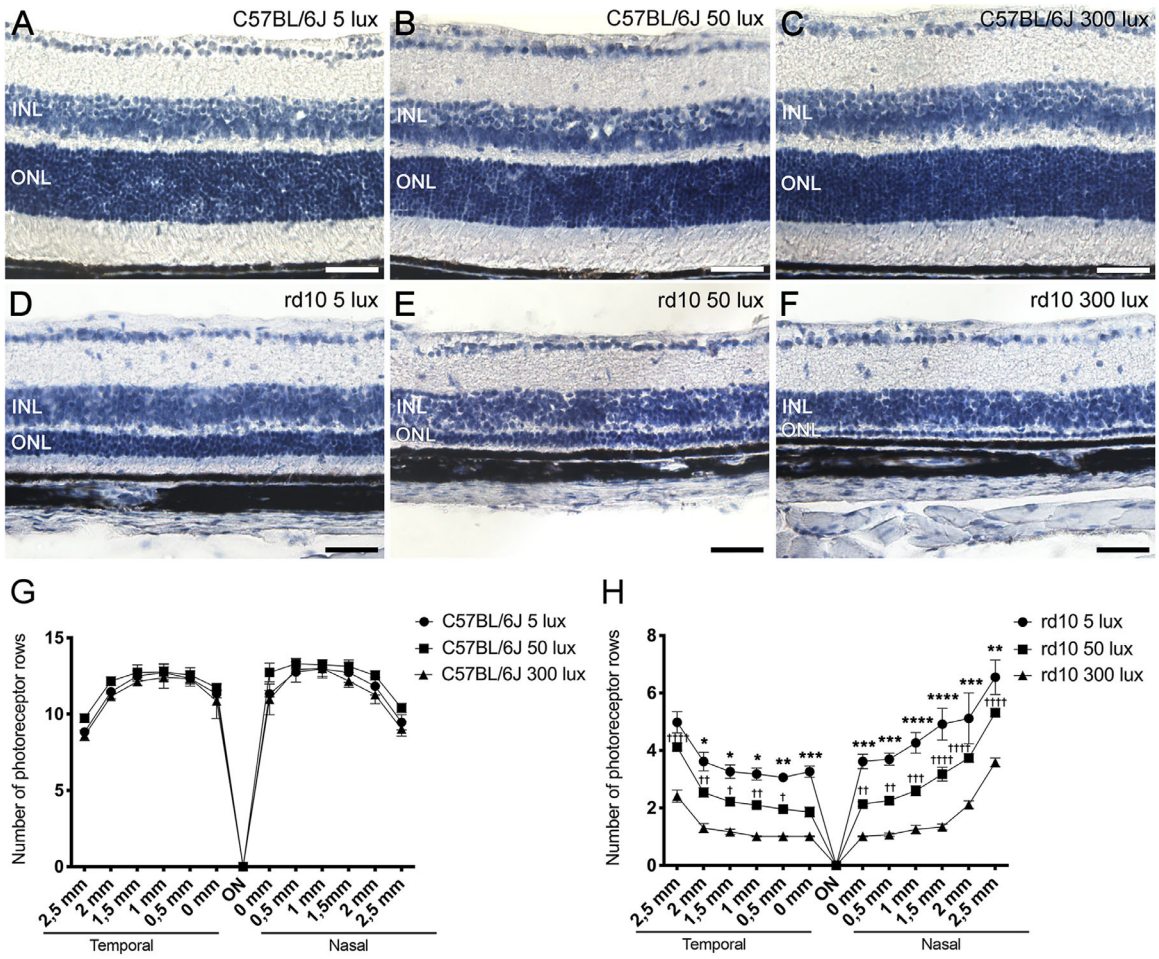

Figure 4. Effect of environmental light conditions on outer nuclear layer. (**A–F**) Cross-sectional cryosections of retinas from P30 C57BL/6J mice (**A–C**) and rd10 mice (**D–F**) maintained under 5, 50, and 300 lux cyclic light. Images correspond to the central area of the retina, near the optic nerve. (**G**, **H**) Mean number of photoreceptor rows along central sections of the retina from C57BL/6J mice (**G**) and rd10 mice (**H**) reared under the different light conditions ($n = 3$ to 7). Two-way ANOVA and Tukey's post hoc test. $^{*}P < 0.05$, $^{**}P < 0.01$, $^{***}P < 0.001$, $^{****}P < 0.0001$ for comparisons between animals housed at 50 and 300 lux. $^{\dagger}P < 0.05$, $^{\dagger\dagger}P < 0.01$, $^{\dagger\dagger\dagger}P < 0.001$, $^{\dagger\dagger\dagger\dagger}P < 0.0001$ for comparisons between animals housed at 5 and 50 lux. INL, inner nuclear layer; ONL, outer nuclear layer; ON, optic nerve. *Scale bars*: 50 µm.

also progressively accumulated in the cell body as the ambient light intensity became higher (Figs. 5G–5I). Also, cones of rd10 mice reared at 5 lux (Figs. 5D, 5J) presented short and swollen outer segments and drastically reduced axon length. When the housing light intensity was higher, cones completely lost their axons, and pedicles emerged directly from the cell body (rd10 mice at 50 lux) (Figs. 5E, 5K). Cone morphology had completely degenerated in rd10 mice reared at 300 lux, when the cell body was the only identifiable structure (Figs. 5F, 5L).

Light-Induced Degeneration of Photoreceptor Synaptic Connectivity

When the outer retina is damaged, postsynaptic cells are also involved in remodeling processes. In order to analyze synaptic connectivity between photoreceptors and postsynaptic horizontal cells, calbindin was used as a specific marker of horizontal cells and vesicular glutamate transporter 1 (VGluT1) to visualize photoreceptor synaptic boutons. Additionally, C-terminal binding protein 2 (CtBP2) was used as a surrogate marker of presynaptic structures located in photoreceptor axon terminals. No differences in synaptic connectivity were observed among the C57BL/6J experimental groups (5, 50, and 300 lux). As observed in Figures 6A and 6E, C57BL/6J horizontal cells (green) exhibited extensive dendritic and axon terminal tips projecting from the cellular body and coming into contact with the axon terminals of cones and rods. In contrast, a light-dependent remodeling of horizontal cells was noticed in rd10 animals exposed to the three housing light intensities (Figs. 6B–6D, 6F–6H). A drastic reduction in the terminal tips of horizontal cells was observed in rd10 mice raised at 5 lux (Fig. 6F). The rd10 mice maintained at 50 lux showed an even greater retraction of the dendrites and axon terminals of horizontal cells, exhibiting few remaining terminal tips (Fig. 6G) and sending those remaining processes toward the inner nuclear layer, as observed in rd10 mice raised at 300 lux (Fig. 6H). Moreover, a light-intensity-dependent reduction in VGluT1 staining was found in rd10 mice (Figs. 6J–6L) compared to C57BL/6J counterparts (Fig. 6I), evidencing a loss of functional axon terminals of photoreceptors. Likewise,

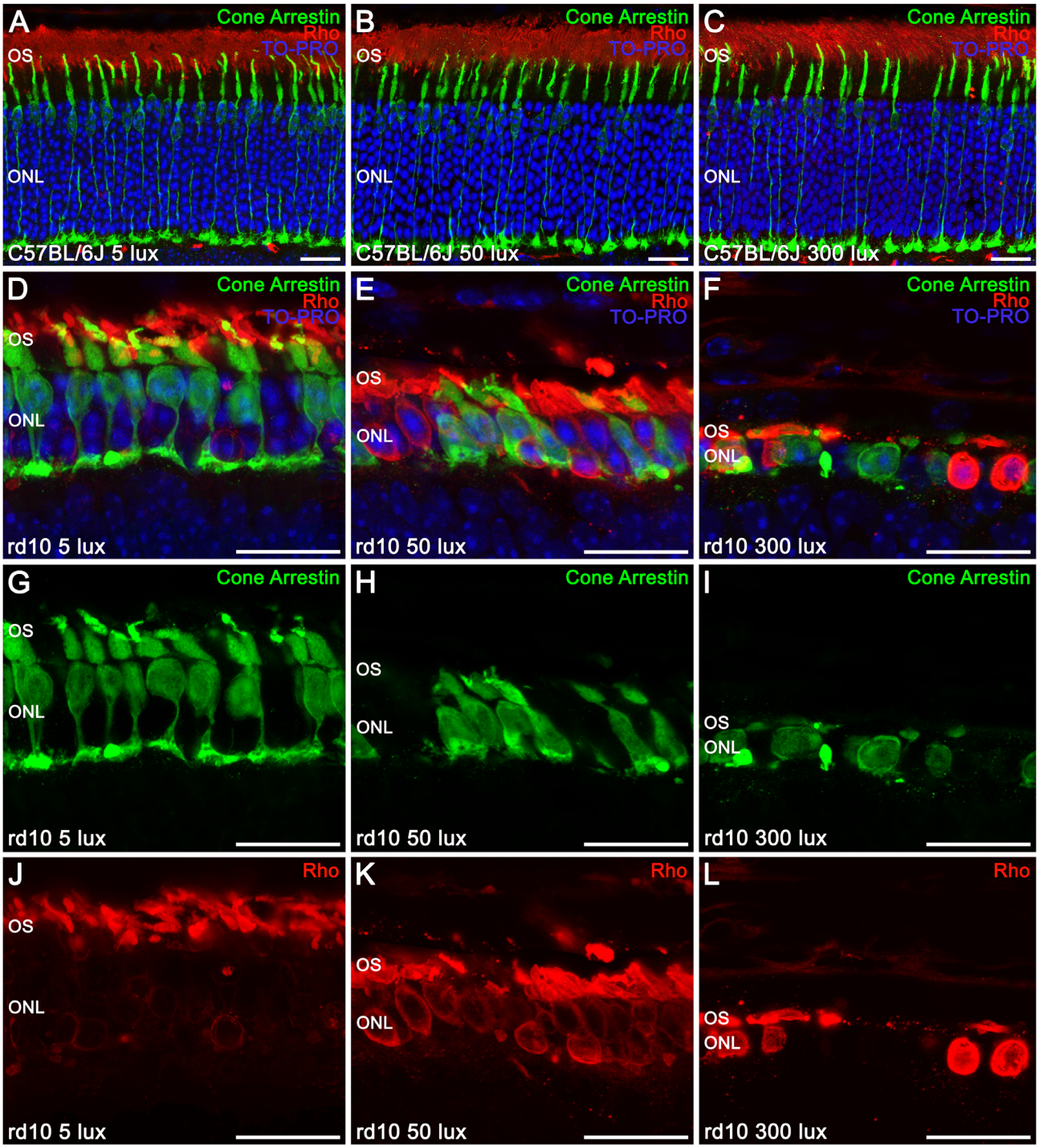

Figure 5. Effect of environmental light conditions on photoreceptor morphology. (**A–L**) Cross-sectional cryosections of retinas from P30 C57BL/6J mice (**A–C**) and rd10 mice (**D–L**) reared under 5, 50, and 300 lux cyclic light and immunolabeled against cone arrestin (cone cells, *green*), rhodopsin (Rho, rod cells, *red*), and TO-PRO 3 (nuclei, *blue*). In C57BL/6J mice, merged images showed a normal cone photoreceptor morphology and rhodopsin distribution (**A–C**). In rd10 mice, merged images (**D–F**) showed a light-dependent degeneration of the photoreceptors, with an abnormal distribution of rhodopsin (**G–I**) accumulated in the rod cell body and a progressive morphological alteration of the cones (**J–L**). OS, outer segments; ONL, outer nuclear layer. *Scale bars*: 20 µm.

a dramatic loss of synaptic ribbons was observed in rd10 mice depending on the rearing light intensity (5, 50, or 300 lux) (Figs. 6P–6R) and compared to C57BL/6J control mice (Figs. 6M–6O).

The density of presynaptic structures in the OPL was quantified by obtaining the profile plots of mean gray intensity for retinal sections stained with CtBP2 (Figs. 6M–6R). No differences were found between the C57BL/6J

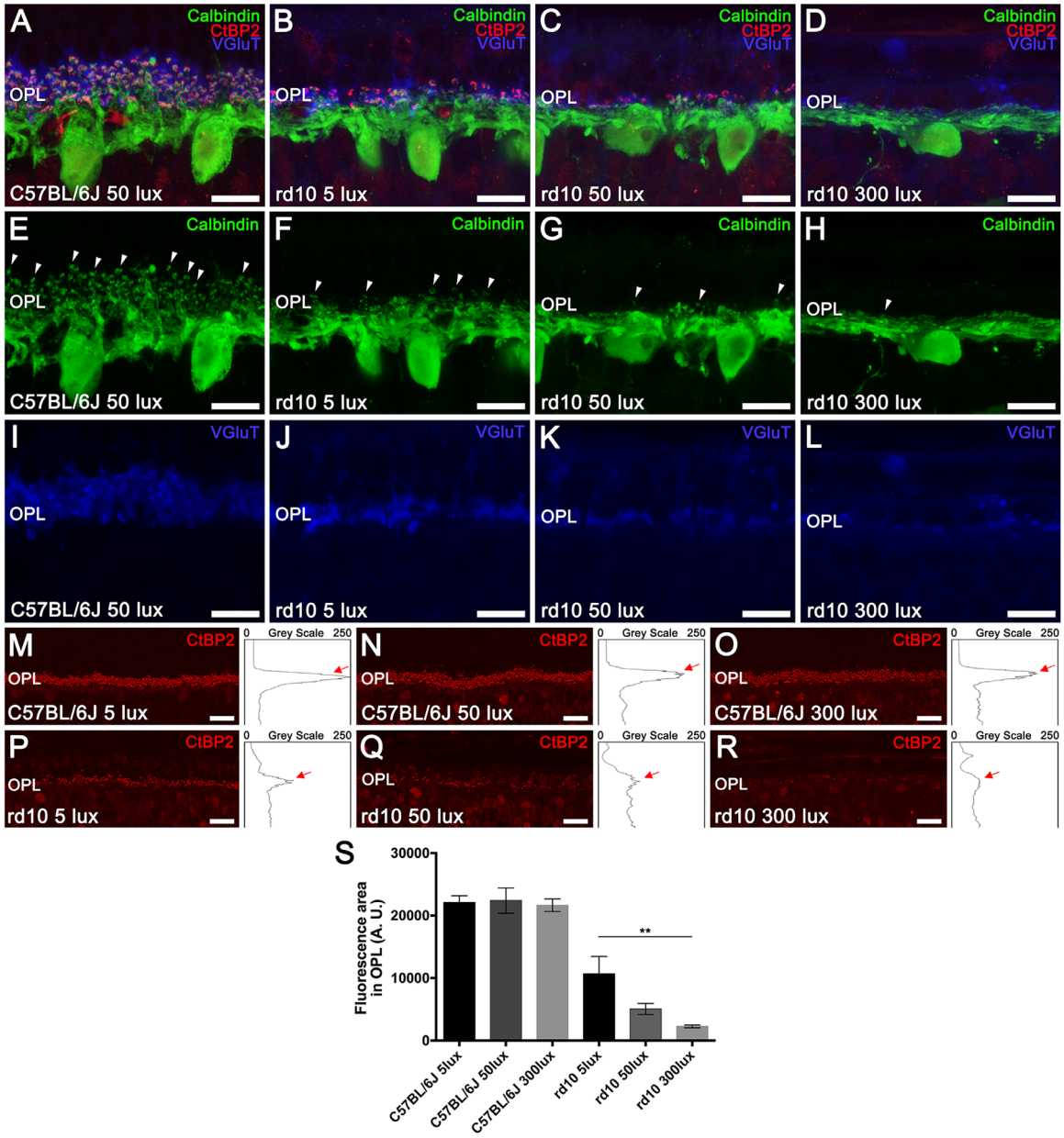

Figure 6. Effect of environmental light conditions on photoreceptor connectivity and second-order neurons. (**A–L**) Cross-sectional cryosections of retinas from a representative C57BL/6J mouse maintained at 50 lux cyclic light (**A**, **E**, **I**) and rd10 mice (**B–D**, **F–H**, **J–L**) reared at 5, 50, and 300 lux cyclic light. Retinas were immunolabeled against calbindin (horizontal cells, *green*), VGluT (axon terminals, *blue*), and CtBP2 (presynaptic structures, *red*). Merged images showed a light-dependent degeneration of synaptic connectivity between photoreceptors and their second-order neurons in rd10 mice (**B–D**) compared with the C57BL/6J mouse retina (**A**). (**E–H**) Calbindin immunolabeling revealed a progressive light-dependent degeneration of the dendritic arborization of the horizontal cells in rd10 mice. *Arrowheads* point to conserved horizontal cell tips. (**I–L**) VGluT immunolabeling evidenced a light-dependent loss of functional photoreceptor axon terminals in rd10 mice. (**M–R**) Representative cross-sectional retinal cryosections showing CtBP2 immunolabeling and the corresponding profile plots of mean gray intensity from C57BL/6J (**M–O**) and rd10 mice (**P–R**) reared at the different light conditions. *Red arrows* point to CtBP2 peaks at the OPL level. (**S**) Quantification of CtBP2 fluorescence at the OPL level for each experimental group ($n = 3$), showing a light-dependent reduction in rd10 mice. OPL, outer plexiform layer. Kruskal–Wallis and Dunn's post hoc test. $^{**}P < 0.01$. *Scale bars*: 10 µm (**A–L**), 20 µm (**M–R**).

mice at different light conditions (Fig. 6S). By contrast, the mean area of the profiles obtained at the OPL significantly decreased in rd10 mice housed at 5, 50, and 300 lux compared to the corresponding C57BL/6J animals (52%, 77%, and 90% lower, respectively). When comparing rd10 mice groups, a significant light-dependent reduction of the mean area of the profiles was observed ($P < 0.005$), where animals reared at 300 lux showed the lowest mean area (Fig. 6S), which was significantly lower than the one from rd10 mice housed at 5 lux (79% lower, $P < 0.01$).

Light-Dependent Increase of Inflammation Markers

During retinal degeneration, inflammatory processes are triggered. Flow cytometry analysis of retinal cells allowed

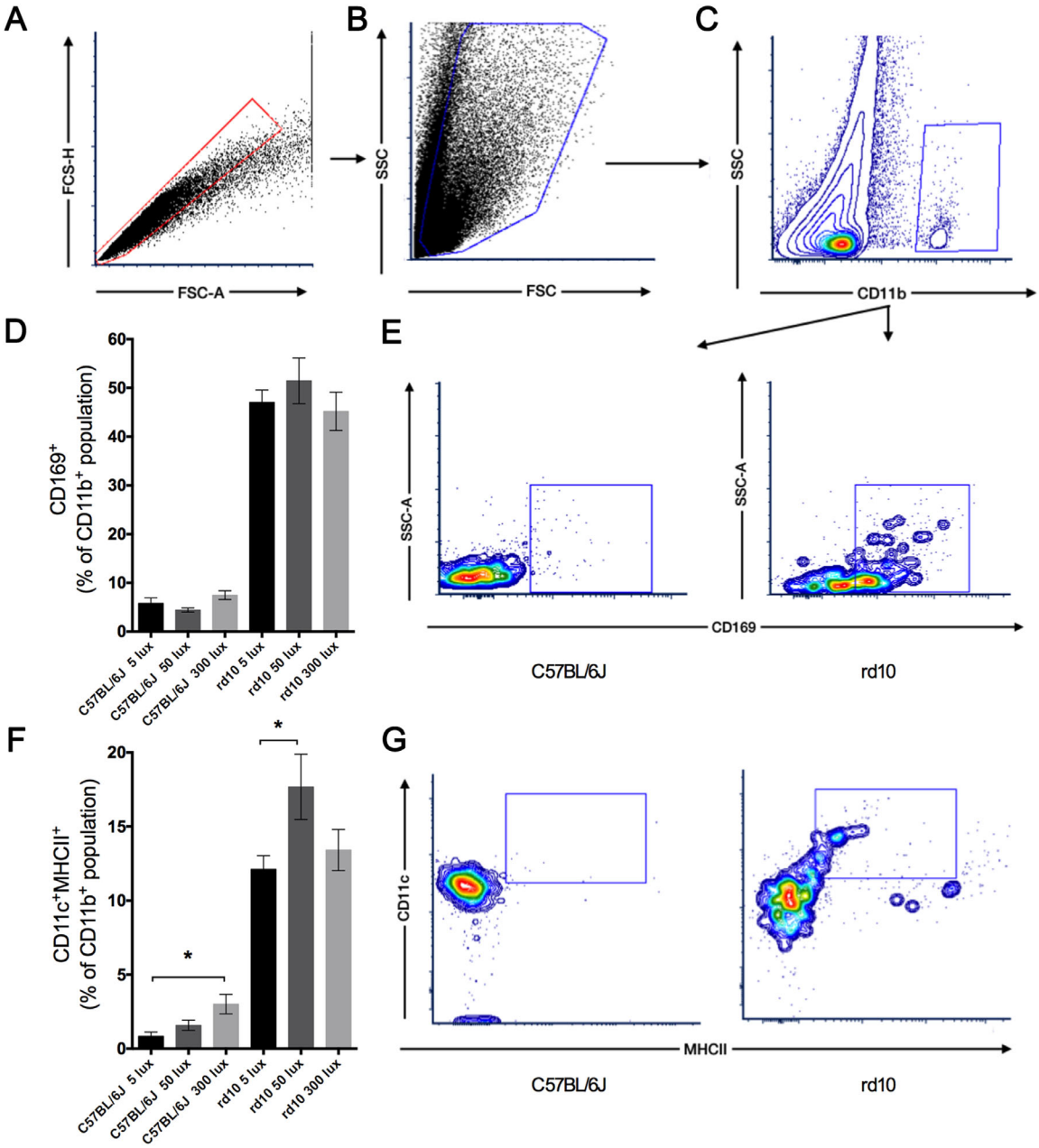

Figure 7. Effect of environmental light conditions on inflammatory cells. (**A**–**C**) Whole retinal cells from C57BL/6J and rd10 mice reared at 5, 50, and 300 lux cyclic light stained for CD11b, CD45, CD11c, MHC class II, and CD169 and analyzed by flow cytometry. After gating singlets (**A**) and discarding cell debris (**B**), $CD11b^+$ cells were gated (**C**) and analyzed. (**D**, **E**) Mean values of $CD169^+$ populations for C57BL/6J and rd10 mice at different light conditions (**D**) and representative contour plots of CD169 expression (**E**). (**F**, **G**) Mean values of $CD11c^+$–MHC class II^+ populations from C57BL/6J and rd10 mice at different light conditions (**F**) and representative plots presenting CD11c and MHC class II expression (**G**). Each dot plot is representative of a minimum of four independent replicates. Kruskal–Wallis and Dunn's post-hoc test. $^*P < 0.05$.

differentiating among the immune-related cell populations implicated in the degenerative process. As expected, positive staining of the markers CD11b and CD45 showed a significant rise in retinas from rd10 mice compared to C57BL/6J mice. After excluding doublets (Fig. 7A) and cellular debris (Fig. 7B), CD11b-positive populations (Fig. 7C) were analyzed for their immunoreactivity against CD169 (Fig. 7D) or against CD11c and MHC class II (Fig. 7F) antigens. Although the number of $CD11b^+$–$CD169^+$ cells was significantly higher in rd10 mice than in their C57BL/6J mice counterparts at all conditions tested, no significant differences were observed between different light intensities in rd10 mice (Figs. 7D, 7E). A significant increase of activated immune-related cells ($CD11b^+$–$CD11c^+$–MHC class II^+) was observed in rd10 mice compared to control mice at all conditions tested (Fig. 7G). Moreover, in rd10 mice maintained at 50 lux this cell population was significantly higher than that observed in mice at 5 lux ($P < 0.05$) (Fig. 7F). Finally, C57BL/6J mice showed an increase of the $CD11b^+$–$CD11c^+$–MHC class II^+ cell population that correlated with

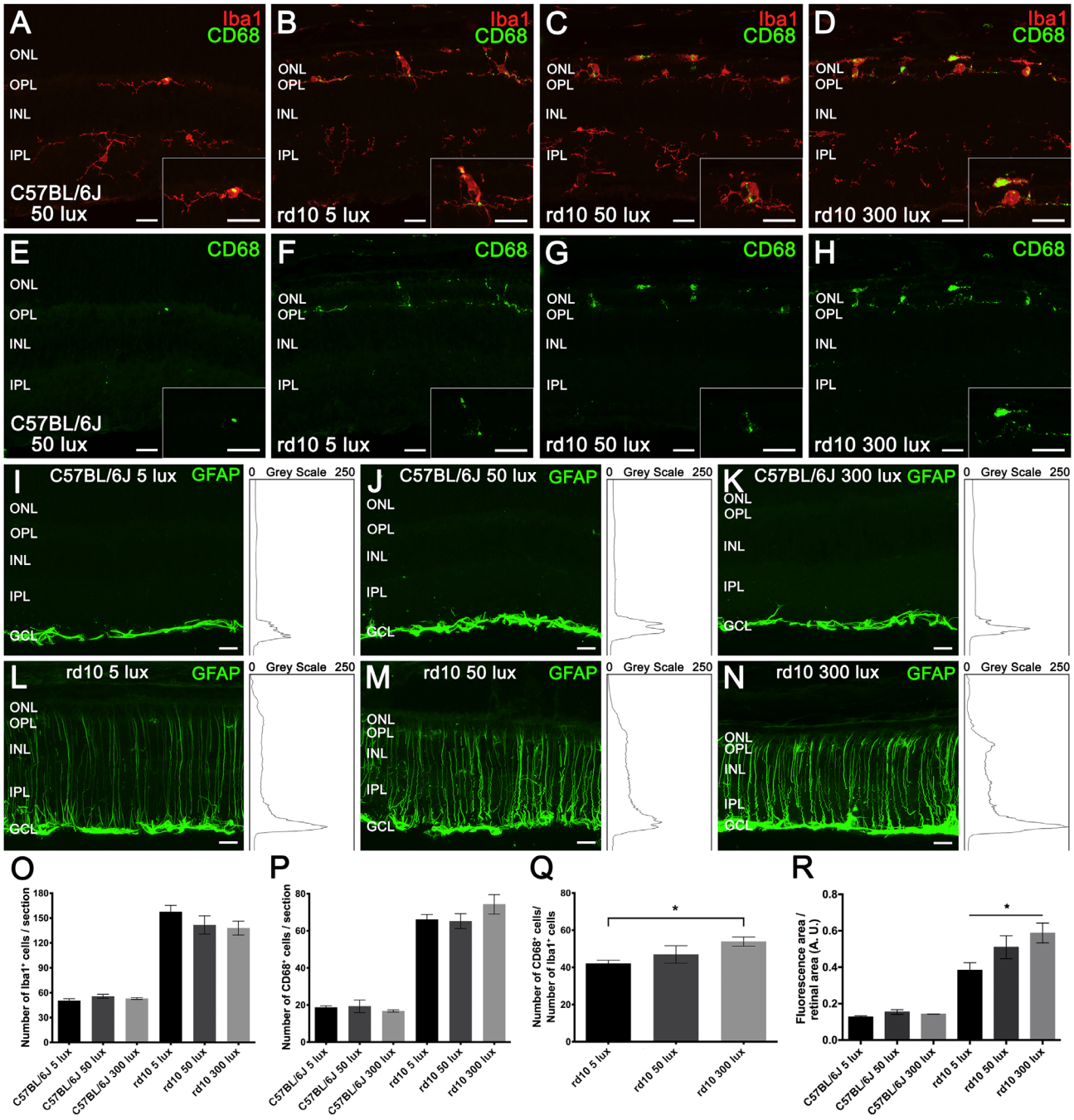

Figure 8. Effect of environmental light conditions on retinal microglia and macroglia. (**A–H**) Representative images of retinal sections from a C57BL/6J mice maintained at 50 lux cyclic light (**A**, **E**) and rd10 mice reared at 5 (**B**, **F**), 50 (**C**, **G**), and 300 lux (**D**, **H**) cyclic light, immunolabeled against Iba1 (microglia, *red*) and CD68 (phagocytic vesicles, *green*). CD68 immunolabeling revealed a light-dependent increase in phagocytic activity of microglial cells in rd10 mice (**F–H**). Insets show a magnification of representative microglial cells. (**I–N**) Representative cross-sectional retinal cryosections showing GFAP immunostaining (activated macroglia, *green*) and their corresponding profile plots of mean gray intensity from C57BL/6J mice (**I–K**) and rd10 mice (**L–N**) reared at 5, 50, and 300 lux. GFAP immunolabeling showed a light-dependent increase in reactive gliosis in rd10 mice (**L–N**). (**O–Q**) Quantification of the number of Iba1$^+$ cells (**O**) and CD68$^+$ cells (**P**) per section from each experimental group and the CD68$^+$/Iba1$^+$ ratio (**Q**) for rd10 mice ($n = 4$ to 6). (**R**) Quantification of GFAP immunofluorescence relativized to the retinal area for each experimental group ($n = 3$). Kruskal–Wallis and Dunn's post-hoc test. $^*P < 0.05$. ONL, outer nuclear layer; OPL, outer plexiform layer; INL, inner nuclear layer; IPL, inner plexiform layer. *Scale bar*: 20 µm.

the increment of light intensity, showing statically significant differences between mice housed at 5 lux and those at 300 lux ($P < 0.05$) (Fig. 7F).

To further analyze the participation of activated microglial cells in the light-intensity-dependent inflammation process, Iba1$^+$ populations and immunoreactivity against the CD68 marker, evidence of phagocytic activity, were assessed in retinal sections from each experimental group (Figs. 8A–8H). Immunohistochemistry images showed an increase in Iba1$^+$ cells (red) and CD68$^+$ cells (green)

in rd10 mice (Figs. 8B–8D, 8F–8H) compared to C57BL/6J animals (Figs. 8A, 8E). Also, these cells migrated toward the photoreceptor layers (ONL and outer segments) in rd10 mice retinas, unlike the C57BL/6J animals, where no Iba1$^+$ cells could be detected above the OPL. In the rd10 mice retinas, an increase was observed in the number of microglia with an ameboid shape and phagocytic profile as the light intensity increased. The quantification of immune-related cells showed a significant increase in both the Iba1$^+$ (Fig. 8O) and the CD68$^+$ (Fig. 8P) cell populations in rd10 mice ($P < 0.01$ and $P < 0.05$, respectively) as compared to C57BL/6J animals. No differences among C57BL/6J groups or among rd10 groups were found. However, CD68$^+$/Iba1$^+$ cell ratios (Fig. 8Q) showed a gradual increment in rd10 mice as the light intensity increased, being statistically significant between 5 and 300 lux intensity ($P < 0.05$). This indicates that the activation degree of microglial cells depends on the light intensity in the rd10 degeneration.

The reactive gliosis of macroglial cells (astrocytes and Müller cells) was analyzed by quantifying GFAP immunoreactivity in retinal sections from each experimental group. No differences were observed between C57BL/6J mice reared at different light conditions (Figs. 8I–8K), in which GFAP immunoreactivity was only detectable in the inner margin of the retina, where astrocytes are located (Figs. 8I–8K). By contrast, GFAP immunoreactivity increased in rd10 mice (Figs. 8L–8N), compared to their control C57BL/6J animals (Figs. 8I–8K) (at least 50% higher). Furthermore, a light-dependent significant increase in reactive gliosis was observed in rd10 animals housed at the different conditions (Fig. 8R), as the GFAP immunoreactivity in animals reared at 300 lux was higher than that of rd10 mice housed at 5 lux ($P < 0.05$). The retinas of these mice showed GFAP immunoreactivity not only in the inner margin of the retina but also throughout the entire Müller cell length (Figs. 8L–8N), which also suffered a progressive shortening.

Light-Induced Changes in Oxidative Stress Biomarkers

Retinal oxidative stress was analyzed in each experimental group by measuring protein levels of both neuronal nNOS, involved in the production of RNS, and 4-HNE, indicative of lipid peroxidation, by western blotting. Also, the RCVRN protein level, which is proportional to the number of photoreceptor cells, was measured. All western blot measurements were first normalized by GAPDH as a protein loading control and later normalized per the amount of RCVRN detected. Although retinas from the three C57BL/6J mice groups showed no differences in levels of RCVRN (Figs. 9A, 9B), the rd10 mice retinas showed a light-dependent decrease (Figs. 9C, 9D) that correlated with the loss of photoreceptor cells in these animals. Normalized levels of the analyzed oxidative biomarkers did not change between retinas from C57BL/6J animals housed in different light conditions (Figs. 9E, 9F), but a light-dependent increase in the normalized levels of 4-HNE (Fig. 9G) and nNOS (Fig. 9H) was found in retinas from rd10 mice, with a statistically significant increment in retinal nNOS protein expression ($P < 0.05$).

To confirm western blot results and to evaluate intracellular ROS in situ, we used the DHE probe, which is a sensitive marker of the superoxide anion levels. Considering that the greatest differences in oxidative stress measured by 4-HNE and nNOS were observed between animals reared at 50 and 300 lux, intracellular superoxide anion levels were assessed in these experimental groups. Whole-mount retinas from rd10 mice (Fig. 9J) showed higher immunoreactivity at the photoreceptor layer than that observed in C57BL/6J animals (Fig. 9I), which showed only a few marked cells. Quantification of the number of photoreceptor cells that presented fluorescence emission of oxidized DHE per retinal area showed no significant differences between C57BL/6J mice reared at 50 and 300 lux (Fig. 9K). By contrast, the number of cells showing fluorescence emission was drastically higher in rd10 mice reared at 50 and 300 lux compared to their corresponding C57BL76J mice (more than 3000 and 10,000% higher, respectively) (Fig. 9K). Moreover, a significant light-dependent increase ($P < 0.0001$) in the number of fluorescent cells was observed in rd10 mice housed at 300 lux as compared to the rd10 mice housed at 50 lux (Fig. 9K).

Discussion

It has been demonstrated that complete light deprivation may exert a neuroprotective effect on the progression of RP, whereas exposure to light can damage retinal cells.[25,27,48] In many studies, retinal degeneration has been assessed by testing a single light intensity or complete darkness.[9,25,27,49] In this study, we evaluated whether slight changes in light-intensity conditions may affect the rate of the neurodegeneration process in RP, using the rd10 mouse model. One of the main novelties of this study compared to other published works is the analysis of three lighting conditions, which represented the three categories of vision: scotopic, very low levels of lighting (5 lux); mesopic, low levels of lighting (50 lux); and photopic, indoor illumination conditions (300 lux). Our results demonstrate that the evolution of the neurodegenerative process in RP changes depending on the intensity of lighting conditions, indicating that scotopic, mesopic, and photopic light conditions are directly involved in the rate of degeneration in RP. It should be considered that ~50 lux or ~300 lux are the commonly used rearing light intensities for rd10 animals[5,6,25,50–53] when lighting conditions are specified in the literature.

Previous studies showed that an amino acid variation at the position 450 of RPE65 protein (*Leu$_{450}$Met*) confers resistance against light-induced damage, which has been described in C57BL/6J mouse.[29,54,55] RPE65 is a protein expressed in the retinal pigment epithelium and is involved in the rhodopsin regeneration during the visual cycle. It was also found that the animal strains carrying the variation *Rpe65Met$_{450}$* present lower levels of RPE65 protein and a slower visual cycle.[20,29,54,55] In the present study, we have shown that the rd10 mouse also carries the same variation (*Rpe65Met$_{450}$*). Nevertheless, our results show a drastic loss of retinal responsiveness in rd10 mice at the endpoint of the study, which correlates with the severe morphological changes observed, mainly affecting the outer retina, where a dramatic reduction in the number of photoreceptor cells was found. Interestingly, these changes were different for rd10 mice reared at different light intensities, with worse functional and morphological outcomes observed in mice reared at the highest light intensity (300 lux). The fact that rd10 mice housed at 5 lux had better preserved retinal function and structure agrees with previous studies showing that dark-adapted animals suffering from RP exhibited a slower rate of degeneration compared with light-exposed

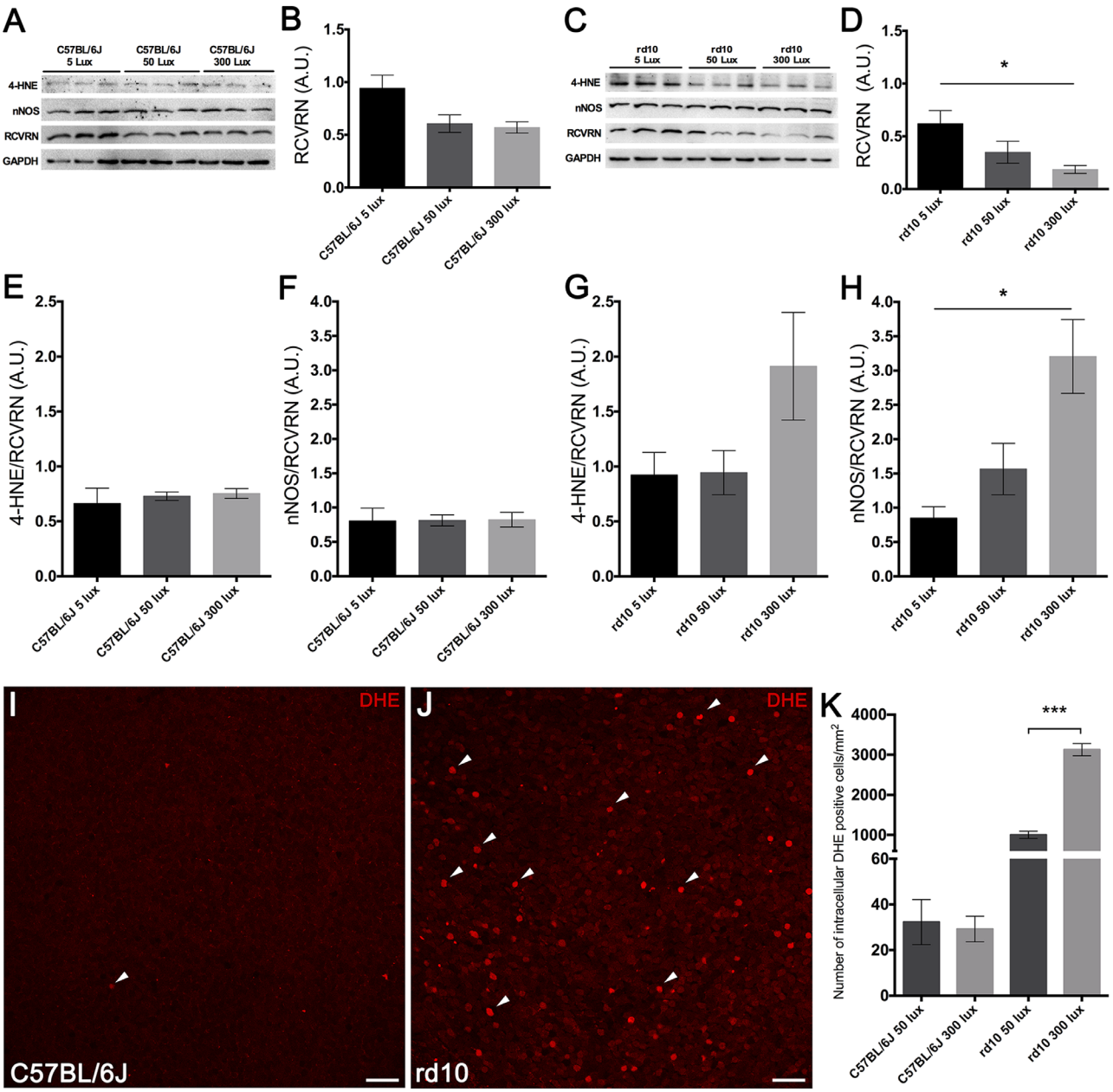

Figure 9. Effect of environmental light conditions on oxidative stress. (**A–H**) Representative western blots (**A**, **C**) and protein level quantification (**B**, **D**, **E–H**) of 4-HNE, nNOS, RCVRN, and GAPDH in C57BL/6J mice (**A**, **B**, **E**, **F**) and rd10 mice (**C**, **D**, **G**, **H**) reared at 5, 50, and 300 lux cyclic light. Mean RCVRN levels in C57BL/6J mice (**B**) and rd10 mice (**D**), normalized to GAPDH expression, revealed a light-dependent reduction in rd10 mice. Expression of 4-HNE and nNOS was normalized to RCVRN levels. Expression of both 4-HNE and nNOS exhibited a light-dependent increase in oxidative stress in rd10 mice. (**I–J**) Images from whole-mounted retinas showing the immunoreactivity of DHE probe at the photoreceptor level in a representative C57BL/6J mouse (**I**) and a representative rd10 mouse (**J**) reared at 50 lux cyclic light. *Arrowheads* point to intracellular DHE-positive cells. (**K**) Quantification of intracellular DHE-positive cells per mm^2 in C57BL/6J and rd10 mice reared at 50 and 300 lux cyclic light. Kruskal–Wallis and Dunn's post hoc test; Mann–Whitney *U* test. $^{*}P < 0.05$, $^{***}P < 0.01$. *Scale bars*: 20 µm.

animals.[9,27,48] As the results of Sundar et al.[9] show, the retina of rd10 mice kept in total darkness also degenerates, remaining approximately four photoreceptors rows in the ONL at P45, being probably slightly more preserved than our results found in rd10 mice housed at 5-lux illumination. Nevertheless, the absence of a dark-reared rd10 mice experimental group in our study may be a limitation to better determining the threshold of light-induced retinal degeneration in rd10 mice.

The photoreceptor degeneration in rd10 mice has been extensively studied since this animal model emerged; however, there are some discrepancies with regard to the rate of photoreceptor degeneration described by various authors. Barhoum et al.[5] and Gargini et al.[50] reported that photoreceptor degeneration in rd10 mice began around P20, with the maximum degeneration occurring around P25 when animals were raised at an illumination of around 50 to 60 lux. In contrast, Arango-Gonzalez et al.[51] and Roche

et al.[35] showed that the peak of photoreceptor death in the same mice strain was around P18 to P20. However, these authors did not indicate the light-intensity conditions under which the animals were raised. Because the rearing light intensity affects the rate of photoreceptor degeneration in rd10 mice, it seems important that the light conditions should be standardized among the different research groups. This is especially relevant when it comes to comparing the effectiveness of possible therapies. Our results also show a marked remodeling in the horizontal cell processes and a light-dependent loss of the synaptic contacts between the photoreceptor terminals and the horizontal cell processes in rd10 mice. These findings correlate with previous ones showing advanced stages of retinal degeneration in rd10 mice[5,50,56] and with the described process of retinal remodeling during photoreceptor degeneration.[5,10,57–62]

In all retinal degenerative diseases, photoreceptor degeneration is accompanied by the proliferation and activation of resident microglia and by the recruitment of immune cells as monocytes and macrophages, which contribute to the inflammatory state of the tissue.[10,31,33] Accordingly, our results show an increase in the immune cells implicated in the inflammatory process in rd10 mice. However, rd10 mice raised in different light conditions showed few differences in the immune-related cells populations, probably due to the advanced state of the degenerative process at the endpoint of the study (P30). Nevertheless, the microglial cells acquire an ameboid shape, and their phagocytic activity increases in a light-intensity-dependent manner. The activation of retinal Müller cells and astrocytes, referred to as reactive gliosis, is also a common feature in rd10 mice.[50,56] Here, we show that there is a light-intensity-dependent increase in reactive gliosis in rd10 mice, together with a progressive light-intensity-dependent reduction in the length of Müller cells, which has been associated with the degeneration of photoreceptor cells.[50,56]

The main mechanisms involved in the exacerbation of retinal degeneration are not yet known in detail. Our results point to the increase of oxidative stress as one of the possible mechanisms underlying gradual light-induced photoreceptor degeneration, as a gradual increase of RNS and ROS was observed when the environmental light intensity was higher during light time. This finding coincides with previous work that has described an increase in retinal ROS photosynthesized from different sources[63–65] when using blue light. In the retina, RNS have an important role in the increment of oxidative stress.[66] Specifically, nNOS is the main source of NO in photoreceptors and contributes to the generation of RNS.[66] Thus, the correlation between photoreceptor loss and nNOS protein levels observed in rd10 mice exposed to different light conditions possibly implicates RNS in the onset and exacerbation of photoreceptor degeneration. In addition to light-induced changes in RNS, our results showed a drastic light-intensity-dependent increase of intracellular superoxide anions in rd10 mice. Moreover, the increase in both RNS and superoxide anions correlated with a relative, although non-significant, increase in 4-HNE, which is known as the major diffusible toxic product generated by lipid peroxidation.[11] It should also be noted that slight non-significant increases in oxidative stress were observed in a light-dependent manner in C57BL/6J mice, although these changes are not relevant enough to trigger photoreceptor death in these animals. Probably, the increase in RNS, 4-HNE, or superoxide anions in C57BL/6J mice is compensated by the antioxidant mechanisms that healthy retinas activate in response to homeostasis disruption.[67,68] By contrast, when basal oxidative stress is relatively high, due to the disease process, light-induced changes in the redox balance probably lead to exacerbation of the retinal degenerative process. On the other hand, the increase of 4-HNE adducts in a light-intensity-dependent manner, due to oxidatively damaged lipids, could be directly related to inflammation[69–71] and cell death[72–74] in rd10 mice. It is important to keep in mind that rd10 mice have a mutation in the *Pde6b* gene that causes an accumulation of cGMP and keeps cGMP-gated cation channels open, generating an excessive accumulation of cations within the cell and inducing oxidative stress and photoreceptors degeneration.[7–9,75]

One commonly proposed hypothesis that explains retinal photodamage is based on the light-induced accumulation of all-*trans*-retinal, one of the products of the phototransduction cascade. The processing of all-*trans*-retinal and its transformation back into the 11-*cis*-retinal chromophore is essential for the survival of photoreceptors.[20,76,77] The accumulation of free all-*trans*-retinal within photoreceptors mediates the production of oxidative stress through the generation of superoxide radicals and other ROS when the light continues irradiating these photoreceptors.[76,78,79] Nevertheless, other evidence may not support this hypothesis. The all-*trans*-retinal production per eye after rhodopsin photobleaching in mice[80] is significantly lower than the concentration that promotes the death of RPE cultured cells.[81] Moreover, some authors do not consider all-*trans*-retinal to be sufficiently stable and abundant to be the main sensitizer for light-dependent damage.[82,83] Finally, the susceptibility to retinal light damage in rats increases with age,[84] whereas there is no evidence of an age-dependent increment of all-*trans*-retinal.

Another hypothesis recently proposed by Sundar et al.[9] suggests that the light-induced exacerbation of photoreceptors death in the rd10 mice is initiated by a rhodopsin-mediated signaling cascade. By removing the *Rpe65* gene from rd10 mice, they observed that the retina was equally preserved at dark conditions and at light conditions. In contrast, by removing the *Gnat1* gene, which encodes for rod transducin-α, they observed that the retina degenerated under both light and dark conditions. This study indicates that light-induced photoreceptor cell death is mediated by rhodopsin signaling which is transducin independent, affecting cGMP-gated cation channels. These would lead to an accumulation of Ca^{2+} in the cell, inducing photoreceptor degeneration due to oxidative stress.

Likewise, mitochondria are one of the main targets of calcium toxicity[85] and major ROS generators. It has been previously described that light-induced calcium accumulation may result in mitochondrial membrane depolarization and induce a higher production of ROS.[85–87] In addition, it has also been proposed that blue light, which is part of the visible light spectrum, can be absorbed by mitochondrial respiratory chain chromophores, inducing a disruption in mitochondrial dynamics, damaging the mitochondria, and generating an increase in ROS.[88,89] However, considering that mitochondrial chromophores are present in all retinal cells, they may not be the primary agent of light-induced damage, as degeneration occurs primarily in photoreceptor cells.

Finally, it has been demonstrated that lipofuscin fluorophores such as the *bis*-retinoid *N*-retinylidene-*N*-retinylethanolamine (A2E) initiate light-induced apoptosis of RPE cells.[90] These pigments reduce the phagocytic function of these cells[91,92] and are formed in greater quantity when there is an increase in oxygen.[91] Moreover, lipofuscin-related

fundus autofluorescence is increased in retinitis pigmentosa patients.[93] All of this evidence indicates that lipofuscin accumulation could be a possible process that leads to the light susceptibility described in this work.

There is a close relationship among oxidative stress, cell death, and inflammation in neurodegeneration,[94] as well as in retinal diseases.[67,68] Thus, despite identifying the active crosstalk among its main implicated factors,[95,96] it remains difficult to establish which factor is the cause or consequence of the others. Considering the effects attributed to light-induced damage,[77,85,86,97] our results suggest that the increase of oxidative stress could be activating both cell death[15–19] and inflammation pathways.[69–74,98,99] Thus, it seems reasonable that oxidative stress may be one of the underlying mechanisms of the light-induced neurodegeneration in rd10 mice retina, although it may not be the only mechanism. However, more experiments are needed to establish this causation.

Altogether, our results indicate that light-intensity conditions are important for the progression of RP in rd10 mice, even carrying the *Rpe65Met*$_{450}$ variation, as it induced microglia and dendritic cells activation and increased oxidative stress, accelerating the rate of photoreceptor death in the retina and subsequent retinal remodeling, in addition to worsening the visual function. Thus, for proper analysis and interpretation of experimental results, as well as for possible comparison among various studies, rearing light intensity should be considered for RP animal models, and specifically for rd10 mice. Standardization of the lighting conditions would be recommended for rd10 mice and other RP animal models with mutations conferring light-induced retinal degeneration. Moreover, today there is no effective treatment for patients suffering from RP, and protection from light is usually recommended in order to prevent further damage to the retina. As RP is a progressive neurodegenerative disease of the retina where patients become blind, findings from this study indicate that neuroprotection from light-induced damage could be a good option to slow down retinal degeneration in some types of RP.

Acknowledgments

Supported by grants from the Spanish Ministry of Economy and Competitiveness (MINECO-FEDER BFU2015-67139-R); Spanish Ministry of Education (FPU16/04114); Instituto de Salud Carlos III co-financed by European Regional Development funds (RETICS-FEDER RD16/0008/0016); and Asociación Retina Asturias, FARPE-FUNDALUCE, Generalitat Valenciana (PROMETEO/2016/158, ACIF/2016/055 and FEDER IDIFEDER/2017/064).

NC, OK, PL, and VM designed the experiments, analyzed the results, and revised the manuscript. OK, XS-S, EDJ, and NM-G performed the experiments. OK, XS-S, and NM-G analyzed the results and wrote the manuscript. All of the authors approved the manuscript.

Disclosure: **O. Kutsyr**, None; **X. Sánchez-Sáez**, None; **N. Martínez-Gil**, None; **E. de Juan**, None; **P. Lax**, None; **V. Maneu**, None; **N. Cuenca**, None

References

1. Hamel C. Retinitis pigmentosa. *Orphanet J Rare Dis*. 2006;1:40.
2. Hartong DT, Berson EL, Dryja TP. Retinitis pigmentosa. *Lancet*. 2006;368:1795–1809.
3. Danciger M, Blaney J, Gao YQ, et al. Mutations in the PDE6B gene in autosomal recessive retinitis pigmentosa. *Genomics*. 1995;30:1–7.
4. Huang L, Zhang Q, Huang X, et al. Mutation screening in genes known to be responsible for retinitis pigmentosa in 98 small Han Chinese families. *Sci Rep*. 2017;7:1948.
5. Barhoum R, Martínez-Navarrete G, Corrochano S, et al. Functional and structural modifications during retinal degeneration in the rd10 mouse. *Neuroscience*. 2008;155:698–713.
6. Chang B, Hawes NL, Pardue MT, et al. Two mouse retinal degenerations caused by missense mutations in the β-subunit of rod cGMP phosphodiesterase gene. *Vision Res*. 2007;47:624–633.
7. Wang T, Reingruber J, Woodruff ML, et al. The PDE6 mutation in the rd10 retinal degeneration mouse model causes protein mislocalization and instability and promotes cell death through increased ion influx. *J Biol Chem*. 2018;293:15332–15346.
8. Paquet-Durand F, Beck S, Michalakis S, et al. A key role for cyclic nucleotide gated (CNG) channels in cGMP-related retinitis pigmentosa. *Hum Mol Genet*. 2011;20:941–947.
9. Sundar JC, Munezero D, Bryan-Haring C, Saravanan T, Jacques A, Ramamurthy V. Rhodopsin signaling mediates light-induced photoreceptor cell death in rd10 mice through a transducin-independent mechanism. *Hum Mol Genet*. 2020;29:394–406.
10. Cuenca N, Fernández-Sánchez L, Campello L, et al. Cellular responses following retinal injuries and therapeutic approaches for neurodegenerative diseases. *Prog Retin Eye Res*. 2014;43:17–75.
11. Trachsel-Moncho L, Benlloch-Navarro S, Á Fernández-Carbonell, et al. Oxidative stress and autophagy-related changes during retinal degeneration and development. *Cell Death Dis*. 2018;9:812.
12. Bhatt L, Groeger G, McDermott K, Cotter TG. Rod and cone photoreceptor cells produce ROS in response to stress in a live retinal explant system. *Mol Vis*. 2010;16:283–293.
13. King A, Gottlieb E, Brooks DG, Murphy MP, Dunaief JL. Mitochondria-derived reactive oxygen species mediate blue light-induced death of retinal pigment epithelial cells. *Photochem Photobiol*. 2004;79:470–475.
14. Byrne AM, Ruiz-Lopez AM, Roche SL, Moloney JN, Wyse-Jackson AC, Cotter TG. The synthetic progestin norgestrel modulates Nrf2 signaling and acts as an antioxidant in a model of retinal degeneration. *Redox Biol*. 2016;10:128–139.
15. Sanvicens N, Gómez-Vicente V, Masip I, Messeguer A, Cotter TG. Oxidative stress-induced apoptosis in retinal photoreceptor cells is mediated by calpains and caspases and blocked by the oxygen radical scavenger CR-6. *J Biol Chem*. 2004;279:39268–39278.
16. Shen J, Yang X, Dong A, et al. Oxidative damage is a potential cause of cone cell death in retinitis pigmentosa. *J Cell Physiol*. 2005;203:457–464.
17. Yu DY, Cringle SJ. Retinal degeneration and local oxygen metabolism. *Exp Eye Res*. 2005;80:745–751.
18. Carmody RJ, McGowan AJ, Cotter TG. Reactive oxygen species as mediators of photoreceptor apoptosis in vitro. *Exp Cell Res*. 1999;248:520–530.
19. Palamalai V, Darrow RM, Organisciak DT, Miyagi M. Light-induced changes in protein nitration in photoreceptor rod outer segments. *Mol Vis*. 2006;12:1543–1551.
20. Wenzel A, Grimm C, Samardzija M, Remé CE. Molecular mechanisms of light-induced photoreceptor apoptosis and neuroprotection for retinal degeneration. *Prog Retin Eye Res*. 2005;24:275–306.
21. Campochiaro PA, Mir TA. The mechanism of cone cell death in retinitis pigmentosa. *Prog Retin Eye Res*. 2018;62:24–37.

22. Cantó A, Olivar T, Romero FJ, Miranda M. Nitrosative stress in retinal pathologies: review. *Antioxidants*. 2019;8:543.
23. Miranda M, Arnal E, Ahuja S, et al. Antioxidants rescue photoreceptors in rd1 mice: relationship with thiol metabolism. *Free Radic Biol Med*. 2010;48:216–222.
24. Berson EL. Light deprivation for early retinitis pigmentosa. *Arch Ophthalmol*. 1971;85:521–529.
25. Lowe RJ, Daniello KM, Duncan JL, et al. Influence of eye pigmentation on retinal degeneration in P23H and S334ter mutant rhodopsin transgenic rats. *Exp Eye Res*. 2019;187:107755.
26. LaVail MM, Nishikawa S, Steinberg RH, et al. Phenotypic characterization of P23H and S334ter rhodopsin transgenic rat models of inherited retinal degeneration. *Exp Eye Res*. 2018;167:56–90.
27. Paskowitz DM, LaVail MM, Duncan JL. Light and inherited retinal degeneration. *Br J Ophthalmol*. 2006;90:1060–1066.
28. Church DM, Goodstadt L, Hillier LW, et al. Lineage-specific biology revealed by a finished genome assembly of the mouse. *PLoS Biol*. 2009;7:e1000112.
29. Wenzel A, Remé CE, Williams TP, Hafezi F, Grimm C. The Rpe65 Leu450Met variation increases retinal resistance against light-induced degeneration by slowing rhodopsin regeneration. *J Neurosci*. 2001;21:53–58.
30. Noailles A, Kutsyr O, Maneu V, et al. The absence of Toll-like receptor 4 mildly affects the structure and function in the adult mouse retina. *Front Cell Neurosci*. 2019;13:59.
31. Noailles A, Maneu V, Campello L, Lax P, Cuenca N. Systemic inflammation induced by lipopolysaccharide aggravates inherited retinal dystrophy. *Cell Death Dis*. 2018;9:350.
32. Fernández-Sánchez L, Bravo-Osuna I, Lax P, et al. Controlled delivery of tauroursodeoxycholic acid from biodegradable microspheres slows retinal degeneration. *PLoS One*. 2017;12:e0177998.
33. Noailles A, Fernández-Sánchez L, Lax P, Cuenca N. Microglia activation in a model of retinal degeneration and TUDCA neuroprotective effects. *J Neuroinflammation*. 2014;11:186.
34. Roche SL, Kutsyr O, Cuenca N, Cotter TG. Norgestrel, a progesterone analogue, promotes significant long-term neuroprotection of cone photoreceptors in a mouse model of retinal disease. *Invest Ophthalmol Vis Sci*. 2019;60:3221–3235.
35. Roche SL, Wyse-Jackson AC, Byrne AM, Ruiz-Lopez AM, Cotter TG. Alterations to retinal architecture prior to photoreceptor loss in a mouse model of retinitis pigmentosa. *Int J Dev Biol*. 2016;60:127–139.
36. Maruyama K, Ii M, Cursiefen C, et al. Inflammation-induced lymphangiogenesis in the cornea arises from CD11b-positive macrophages. *J Clin Invest*. 2005;115:2363–2372.
37. O'Koren EG, Mathew R, Saban DR. Fate mapping reveals that microglia and recruited monocyte-derived macrophages are definitively distinguishable by phenotype in the retina. *Sci Rep*. 2016;6:20636.
38. Rangaraju S, Raza SA, Li NXA, et al. Differential phagocytic properties of CD45low microglia and CD45high brain mononuclear phagocytes-activation and age-related effects. *Front Immunol*. 2018;9:405.
39. Chidlow G, Ebneter A, Wood JPM, Casson RJ. Evidence supporting an association between expression of major histocompatibility complex II by microglia and optic nerve degeneration during experimental glaucoma. *J Glaucoma*. 2016;25:681–691.
40. Lipski DA, Dewispelaere R, Foucart V, et al. MHC class II expression and potential antigen-presenting cells in the retina during experimental autoimmune uveitis. *J Neuroinflammation*. 2017;14:136.
41. Ronning KE, Karlen SJ, Miller EB, Burns ME. Molecular profiling of resident and infiltrating mononuclear phagocytes during rapid adult retinal degeneration using single-cell RNA sequencing. *Sci Rep*. 2019;9:4858.
42. Jiang H, Lumsden L, Forrester JV. Macrophages and dendritic cells in IRBP-induced experimental autoimmune uveoretinitis in B10RIII mice. *Invest Ophthalmol Vis Sci*. 1999;40:3177–3185.
43. Lehmann U, Heuss ND, McPherson SW, Roehrich H, Gregerson DS. Dendritic cells are early responders to retinal injury. *Neurobiol Dis*. 2010;40:177–184.
44. Tang PH, Pierson MJ, Heuss ND, Gregerson DS. A subpopulation of activated retinal macrophages selectively migrated to regions of cone photoreceptor stress, but had limited effect on cone death in a mouse model for type 2 Leber congenital amaurosis. *Mol Cell Neurosci*. 2017;85:70–81.
45. Linnartz-Gerlach B, Kopatz J, Neumann H. Siglec functions of microglia. *Glycobiology*. 2014;24:794–799.
46. Hughes EH, Schlichtenbrede FC, Murphy CC, et al. Generation of activated sialoadhesin-positive microglia during retinal degeneration. *Invest Ophthalmol Vis Sci*. 2003;44:2229–2234.
47. Martin E, El-Behi M, Fontaine B, Delarasse C. Analysis of microglia and monocyte-derived macrophages from the central nervous system by flow cytometry. *J Vis Exp*. 2017;124:55781.
48. Walsh N, Van Driel D, Lee D, Stone J. Multiple vulnerability of photoreceptors to mesopic ambient light in the P23H transgenic rat. *Brain Res*. 2004;1013:194–203.
49. Li Y, Zhang Y, Chen S, Vernon G, Wong WT, Qian H. Light-dependent OCT structure changes in photoreceptor degenerative rd 10 mouse retina. *Invest Ophthalmol Vis Sci*. 2018;59:1084–1094.
50. Gargini C, Terzibasi E, Mazzoni F, Strettoi E. Retinal organization in the retinal degeneration 10 (rd10) mutant mouse: a morphological and ERG study. *J Comp Neurol*. 2008;500:222–238.
51. Arango-Gonzalez B, Trifunović D, Sahaboglu A, et al. Identification of a common non-apoptotic cell death mechanism in hereditary retinal degeneration. *PLoS One*. 2014;9:e112142.
52. Chang B, Hawes NL, Hurd RE, Davisson MT, Nusinowitz S, Heckenlively JR. Retinal degeneration mutants in the mouse. *Vis Res*. 2002;42:517–525.
53. Samardzija M, Wariwoda H, Imsand C, et al. Activation of survival pathways in the degenerating retina of rd10 mice. *Exp Eye Res*. 2012;99:17–26.
54. Samardzija M, Wenzel A, Naash M, Remé CE, Grimm C. Rpe65 as a modifier gene for inherited retinal degeneration. *Eur J Neurosci*. 2006;23:1028–1034.
55. Wenzel A, Grimm C, Samardzija M, Remé CE. The genetic modifier Rpe65Leu450: effect on light damage susceptibility in c-Fos-deficient mice. *Invest Ophthalmol Vis Sci*. 2003;44:2798–2802.
56. Phillips MJ, Otteson DC, Sherry DM. Progression of neuronal and synaptic remodeling in the rd 10 mouse model of retinitis pigmentosa. *J Comp Neurol*. 2010;518:2071–2089.
57. Cuenca N, Ortuño-Lizarán I, Sánchez-Sáez X, et al. Interpretation of OCT and OCTA images from a histological approach: clinical and experimental implications. *Prog Retin Eye Res*. In press.
58. Jones BW, Marc RE. Retinal remodeling during retinal degeneration. *Exp Eye Res*. 2005;81:123–137.
59. Marc RE, Jones BW, Watt CB, Strettoi E. Neural remodeling in retinal degeneration. *Prog Retin Eye Res*. 2003;22:607–655.
60. Marc RE, Jones BW. Retinal remodeling in inherited photoreceptor degenerations. *Mol Neurobiol*. 2003;28:139–147.
61. Cuenca N, Fernández-Sánchez L, Sauvé Y, et al. Correlation between SD-OCT, immunocytochemistry and functional

findings in an animal model of retinal degeneration. *Front Neuroanat*. 2014;8:151.
62. Pinilla I, Fernández-Sánchez L, Segura FJ, et al. Long time remodeling during retinal degeneration evaluated by optical coherence tomography, immunocytochemistry and fundus autofluorescence. *Exp Eye Res*. 2016;150:122–134.
63. Demontis GC, Longoni B, Marchiafava PL. Molecular steps involved in light-induced oxidative damage to retinal rods. *Invest Ophthalmol Vis Sci*. 2002;43:2421–2427.
64. Wu J, Seregard S, Algvere PV. Photochemical damage of the retina. *Surv Ophthalmol*. 2006;51:461–481.
65. Roehlecke C, Schumann U, Ader M, et al. Stress reaction in outer segments of photoreceptors after blue light irradiation. *PLoS One*. 2013;8:e71570.
66. Krizaj D, Copenhagen DR. Calcium regulation in photoreceptors. *Front Biosci*. 2002;7:d2023–d2044.
67. Nishimura Y, Hara H, Kondo M, Hong S, Matsugi T. Oxidative stress in retinal diseases. *Oxidative Medicine and Cellular Longevity*. 2017;2017:4076518.
68. Masuda T, Shimazawa M, Hara H. Retinal diseases associated with oxidative stress and the effects of a free radical scavenger (edaravone). *Oxid Med Cell Longev*. 2017;2017:9208489.
69. Datta S, Cano M, Ebrahimi K, Wang L, Handa JT. The impact of oxidative stress and inflammation on RPE degeneration in non-neovascular AMD. *Prog Retin Eye Res*. 2017;60:201–218.
70. Valacchi G, Pecorelli A, Cervellati C, Hayek J. 4-hydroxynonenal protein adducts: key mediator in Rett syndrome oxinflammation. *Free Radic Biol Med*. 2017;111:270–280.
71. Yang, H-J, R Hu, Sun H, Chen B, Li X, Chen J-B. 4-HNE induces proinflammatory cytokines of human retinal pigment epithelial cells by promoting extracellular efflux of HSP70. *Exp Eye Res*. 2019;188:107792.
72. Dalleau S, Baradat M, Guéraud F, Huc L. Cell death and diseases related to oxidative stress: 4-hydroxynonenal (HNE) in the balance. *Cell Death Differ*. 2013;20:1615–1630.
73. Sharma A, Sharma R, Chaudhary P, et al. 4-Hydroxynonenal induces p53-mediated apoptosis in retinal pigment epithelial cells. *Arch Biochem Biophys*. 2008;480:85–94.
74. Tanito M, Elliott MH, Kotake Y, Anderson RE. Protein modifications by 4-hydroxynonenal and 4-hydroxyhexenal in light-exposed rat retina. *Invest Ophthalmol Vis Sci*. 2005;46:3859–3868.
75. Sharma AK, Rohrer B. Sustained elevation of intracellular cGMP causes oxidative stress triggering calpain-mediated apoptosis in photoreceptor degeneration. *Curr Eye Res*. 2007;32:259–269.
76. Maeda T, Golczak M, Maeda A. Retinal photodamage mediated by all-trans-retinal. *Photochem Photobiol*. 2012;88:1309–1319.
77. Organisciak DT, Vaughan DK. Retinal light damage: mechanisms and protection. *Prog Retin Eye Res*. 2010;29:113–134.
78. Różanowska M, Sarna T. Light-induced damage to the retina: role of rhodopsin chromophore revisited. *Photochem Photobiol*. 2005;81:1305.
79. Athanasiou D, Aguilà M, Bevilacqua D, Novoselov SS, Parfitt DA, Cheetham ME. The cell stress machinery and retinal degeneration. *FEBS Lett*. 2013;587:2008–2017.
80. Wenzel A, Oberhauser V, Pugh EN, et al. The retinal G protein-coupled receptor (RGR) enhances isomerohydrolase activity independent of light. *J Biol Chem*. 2005;280:29874–29884.
81. Liao Y, Zhang H, He D, et al. Retinal pigment epithelium cell death is associated with NLRP3 inflammasome activation by all-trans retinal. *Invest Ophthalmol Vis Sci*. 2019;60:3034–3045.
82. Noell WK. Possible mechanisms of photoreceptor damage by light in mammalian eyes. *Vis Res*. 1980;20:1163–1171.
83. Hunter JJ, Morgan JIW, Merigan WH, Sliney DH, Sparrow JR, Williams DR. The susceptibility of the retina to photochemical damage from visible light. *Prog Retin Eye Res*. 2012;31:28–42.
84. Organisciak DT, Darrow RM, Barsalou L, et al. Light history and age-related changes in retinal light damage. *Invest Ophthalmol Vis Sci*. 1998;39:1107–1116.
85. Baksheeva VE, Tiulina VV, Tikhomirova NK, et al. Suppression of light-induced oxidative stress in the retina by mitochondria-targeted antioxidant. *Antioxidants (Basel)*. 2019;8:3.
86. Donovan M, Carmody RJ, Cotter TG. Light-induced photoreceptor apoptosis in vivo requires neuronal nitric-oxide synthase and guanylate cyclase activity and is caspase-3-independent. *J Biol Chem*. 2001;276:23000–23008.
87. Maeda A, Maeda T, Golczak M, et al. Involvement of all-trans-retinal in acute light-induced retinopathy of mice. *J Biol Chem*. 2009;284:15173–15183.
88. Tao JX, Zhou WC, Zhu XG. Mitochondria as potential targets and initiators of the blue light hazard to the retina. *Oxid Med Cell Longev*. 2019;2019:6435364.
89. Osborne NN, Núñez-Álvarez C, del Olmo-Aguado S. The effect of visual blue light on mitochondrial function associated with retinal ganglions cells. *Exp Eye Res*. 2014;128:8–14.
90. Sparrow JR, Nakanishi K, Parish CA. The lipofuscin fluorophore A2E mediates blue light-induced damage to retinal pigmented epithelial cells. *Invest Ophthalmol Vis Sci*. 2000;41:1981–1989.
91. Nilsson SEG, Sundelin SP, Wihlmark U, Brunk UT. Aging of cultured retinal pigment epithelial cells: Oxidative reactions, lipofuscin formation and blue light damage. *Doc Ophthalmol*. 2003;106:13–16.
92. Finnemann SC, Leung LW, Rodriguez-Boulan E. The lipofuscin component A2E selectively inhibits phagolysosomal degradation of photoreceptor phospholipid by the retinal pigment epithelium. *Proc Natl Acad Sci U S A*. 2002;99:3842–3847.
93. Kellner U, Kellner S, Weber BHF, Fiebig B, Weinitz S, Ruether K. Lipofuscin- and melanin-related fundus autofluorescence visualize different retinal pigment epithelial alterations in patients with retinitis pigmentosa. *Eye (Lond)*. 2009;23:1349–1359.
94. Chiurchiù V, Orlacchio A, Maccarrone M. Is modulation of oxidative stress an answer? The state of the art of redox therapeutic actions in neurodegenerative diseases. *Oxid Med Cell Longev*. 2016;2016:7909380.
95. Okamoto T, Ozawa Y, Kamoshita M, et al. The neuroprotective effect of rapamycin as a modulator of the mTOR-NF-κB axis during retinal inflammation. *PLoS One*. 2016;11:e0146517.
96. Altmann C, Schmidt MHH. The role of microglia in diabetic retinopathy: inflammation, microvasculature defects and neurodegeneration. *Int J Mol Sci*. 2018;19:110.
97. Tomita H, Tabata K, Takahashi M, Nishiyama F, Sugano E. Light induces translocation of NF-κB p65 to the mitochondria and suppresses expression of cytochrome c oxidase subunit III (COX III) in the rat retina. *Biochem Biophys Res Commun*. 2016;473:1013–1018.
98. Shaw PX, Stiles T, Douglas C, et al. Oxidative stress, innate immunity and age-related macular degeneration. *AIMS Mol Sci*. 2016;3:196–221.
99. Vohra R, Tsai JC, Kolko M. The role of inflammation in the pathogenesis of glaucoma. *Surv Ophthalmol*. 2013;58:311–320.

Investigative Ophthalmology & Visual Science